

Sound wave generation by a spherically symmetric outburst and AGN Feedback in Galaxy Clusters

Xiaping Tang,^{1*} Eugene Churazov,^{1,2}

¹Max Planck Institute for Astrophysics, Karl-Schwarzschild-Str. 1, D-85741 Garching, Germany

²Space Research Institute (IKI), Profsoyuznaya 84/32, Moscow 117997, Russia

Accepted XXX. Received YYY; in original form ZZZ

ABSTRACT

We consider the evolution of an outburst in a uniform medium under spherical symmetry, having in mind AGN feedback in the intra cluster medium (ICM). For a given density and pressure of the medium, the spatial structure and energy partition at a given time t_{age} (since the onset of the outburst) are fully determined by the total injected energy E_{inj} and the duration t_b of the outburst. We are particularly interested in the late phase evolution when the strong shock transforms into a sound wave. We studied the energy partition during such transition with different combinations of E_{inj} and t_b . For an instantaneous outburst with $t_b \rightarrow 0$, which corresponds to the extension of classic Sedov-Taylor solution with counter-pressure, the fraction of energy that can be carried away by sound waves is $\lesssim 12\%$ of E_{inj} . As t_b increases, the solution approaches the ‘slow piston’ limit, with the fraction of energy in sound waves approaching zero. We then repeat the simulations using radial density and temperature profiles measured in Perseus and M87/Virgo clusters. We find that the results with a uniform medium broadly reproduce an outburst in more realistic conditions once proper scaling is applied. We also develop techniques to map intrinsic properties of an outburst (E_{inj} , t_b and t_{age}) to the observables like the Mach number of the shock and radii of the shock and ejecta. For the Perseus cluster and M87, the estimated (E_{inj} , t_b and t_{age}) agree with numerical simulations tailored for these objects with 20 – 30% accuracy.

Key words: galaxies: clusters: intra cluster medium – X-rays: galaxies: clusters – galaxies: active – galaxies: clusters: individual: M87 and Perseus cluster – shock waves

1 INTRODUCTION

The problem of a powerful outburst in a nearly homogeneous medium under spherical symmetry plays an important role in a number of astrophysical contexts, ranging from supernova remnants to AGN feedback in the cores of galaxy clusters. In the latter case, particularly important questions are (i) deriving the energetics of the outburst from readily available observables and (ii) determining what fraction of the outburst energy is going to be thermalized in the gas. They are also the questions that we address in this paper.

The importance of AGN activity on the ICM thermal state in clusters and elliptical galaxies is nowadays widely accepted (e.g., Churazov et al. 2000; McNamara et al. 2000), see e.g., Fabian (2012) and Soker (2016) for reviews. The cooling time of the ICM in cluster cores is short and a source of energy is needed to prevent a massive build up of cold gas and vigorous star formation. This energy is believed to

come from a central supermassive black hole, although the description of the energy transfer from AGN to ICM is still sketchy. Multi-wavelength observations reveal that AGN jets inflate bubbles of relativistic plasma (or at least a mixture of relativistic particles and very hot plasma). When energy is injected in an unperturbed medium, the expanding bubble initially drives a strong shock in the surrounding medium and heats the gas. Later, the bubble expansion becomes subsonic and the shock-heating efficiency drops dramatically. The energy goes instead into the thermal energy of the expanding bubble and PV work. Eventually, bubbles are removed from the cluster core by the buoyancy force. During the process, the rising bubbles must lose their energy after crossing several pressure scale heights (Churazov et al. 2001, 2002; Begelman 2001) and can excite turbulence and/or internal waves that are eventually dissipated into heat (e.g., Zhuravleva et al. 2014). Sound waves could also contribute to the gas heating (e.g., Fabian et al. 2006), if a substantial fraction of energy goes into the waves and they are able to dissipate. Yet another scenario postulates that the bubbles

* E-mail: xt5uv@mpa-garching.mpg.de

are filled with hot, but non-relativistic, plasma and mixing of this plasma with the ICM is the dominant channel for ICM heating (e.g., [Hillel & Soker 2016](#)).

Which of these scenarios dominate depends on the way AGN injects energy to the ICM. While this problem has been addressed in many sophisticated 3D numerical simulations, the uncertainties in choosing the right approximation and parameters precludes unambiguous conclusion. A simpler approach is to use the minimalistic set of assumptions to get order of magnitude constraints on a few of the most important parameters. For instance, one-dimensional (1D) spherically symmetric outburst powered by AGN activity is probably the simplest among all models. It was studied, e.g., in [Forman et al. \(2007, 2017\)](#); [Graham et al. \(2008\)](#); [Randall et al. \(2011\)](#); [Zhuravleva et al. \(2016\)](#) where constraints on the energy/luminosity and duration of the outburst have been obtained. In all these cases the simulations were tailored for a particular object. Several questions arise: (i) are the results obtained for well studied systems universal, (ii) what are the most extreme cases allowed by models, e.g., maximal amount of energy in the form of sound waves, (iii) can one use a few observables to estimate the properties of an outburst without doing actual simulations? To address these question we made a systematic study of an outburst evolution in a very simple setup and derive a scaling needed to apply this analysis to other systems.

In this paper we closely investigate the evolution of an outburst in a low density hot medium under spherical symmetry. Qualitatively, “low density” is assumed to indicate that the radiative energy losses are negligible on time scales of the outburst evolution. The assumption of “hot” means that despite the low density, the thermal pressure in the ambient medium is not negligible and is dynamically important for the expansion of an outburst. Because of the high pressure in the medium, the shock wave driven by the outburst gradually transforms from a strong shock into a weak shock and eventually asymptotically approaches a sound wave as $t \rightarrow \infty$.

In §2, we describe the main assumptions/approximation made in the paper. In §3, we systematically study the evolution of an outburst in uniform medium. In §4, we use the Perseus cluster and M87 as examples to show that the evolution of an outburst in a realistic density and pressure profile of a galaxy cluster does not deviate much from those results in uniform medium. We then develop simple tools to map the observables to the intrinsic properties of an outburst based on simulation with uniform medium. In §5, we create a schematic figure to illustrate the various regimes and physical processes related to the problem of AGN driven outburst and then discuss the physical properties of the outbursts in Perseus cluster and M87. §6 is the conclusion section.

2 OUTLINE OF THE PROBLEM

The primary goal of this paper is to use 1D spherically symmetric outburst model to derive the most basic constraints on the spatial structure and energy partition of AGN driven outbursts in galaxy cluster. Here we outline main assumptions and simplifications made in our discussion.

The initial gas density $\rho_a(r)$ and pressure $P_a(r)$ distributions of the ICM are assumed to be static, where r

is the distance from the cluster center. In the presence of pressure gradients, a balancing force due to gravity is taken into account to maintain hydrostatic equilibrium. Thermal conduction and physical viscosity are neglected for simplification. At age $t_{age} = 0$, energy and mass start to be injected into the center of the cluster. In our simplified problem, for a given $\rho_a(r)$ and $P_a(r)$ profiles of the ICM, the evolution of an outburst is fully determined by its energy and mass injection history. In this paper, we consider simplified energy and mass injection (see Appendix A for a detailed description) which are characterized by three parameters: total injected energy E_{inj} , total injected mass M_{inj} and the duration of the outburst t_b . The adiabatic index of the injected material is γ_{ej} , while the ambient gas has the adiabatic index γ_a . In the context of galaxy clusters, this setup is very similar to the one used in, e.g., [Heinz, Reynolds, & Begelman \(1998\)](#); [Forman et al. \(2007\)](#); [Zhuravleva et al. \(2016\)](#).

The fate of such outbursts could fall into two different evolution tracks depending on the value of the dimensionless ratio $(E_{inj}/M_{inj})/(P_a/\rho_a)$, see Appendix B for detailed discussion. In most astrophysical applications, like the AGN feedback problem studied here, the ratio $(E_{inj}/M_{inj})/(P_a/\rho_a) \gg 1$ and the evolution of the outburst could be divided into three different phases, if we make analogy to instantaneous outburst with $t_b \rightarrow 0$ for outbursts with finite duration time t_b . Based on the relation between the injected energy E_{inj} and mass M_{inj} and the swept up materials thermal energy E_{sw} and mass M_{sw} , the three phases are free expansion phase with $M_{sw} \leq M_{inj}$ and $E_{sw} \ll E_{inj}$, Sedov-Taylor (ST) phase ([Taylor 1946](#); [Sedov 1959](#)) with $M_{sw} > M_{inj}$ and $E_{sw} \leq E_{inj}$, and a wave-like phase with $E_{sw} > E_{inj}$. For the AGN feedback problem of interest here, M_{inj} is unknown from observation but likely to be small, and the free expansion phase is likely to be very brief. So in the rest of the paper, we could simply neglect the injected mass M_{inj} and ignore the free expansion phase which are not very important for our discussion. In view of the weak shock observed in galaxy cluster, we will focus on the transition from ST phase to wave-like phase in this paper.

The transition from ST phase to the wave-like phase happens when the thermal energy of swept up materials E_{sw} becomes comparable with the injected energy E_{inj} . It sets the characteristic length R_E and time t_E of the system, see Appendix C for detail. R_E is the characteristic radius of a sphere such that the total thermal energy of the ICM within the sphere is of order of E_{inj} , i.e.

$$E_{inj} = \frac{4\pi}{3} P_a R_E^3, \quad (1)$$

where we have assumed for simplicity that the pressure $P_a(r) = \text{const.}$ t_E is the sound crossing time of R_E , i.e.

$$t_E = \frac{R_E}{\sqrt{\gamma_a P_a / \rho_a}}. \quad (2)$$

In the subsequent sections, we will study the evolution of an outburst during such transition for different combinations of t_b and t_E . Two special cases that deserve more discussions are (i) the instantaneous outburst with $t_b/t_E \rightarrow 0$ and (ii) the continuous outburst (or “slow piston” mode) with $t_b/t_E \rightarrow \infty$. They behave very differently during the transition from the early ST phase to the late wave-like phase es-

pecially in energy partition. In the first case, a large amount of energy is released during a short period of time. When the energy release quenches, a strong shock still exists which could heat the surrounding ambient gas and generate a significant amount of entropy. We also expect that the state of such an outburst at age $t_{age} \gg t_b$ will not be very sensitive to the actual value of t_b . In the second case, the injected energy is released over a time scale much larger than the characteristic time t_E of the system. As a result, the ejecta always expand subsonically, except for a short interval at early time, and no net entropy generation in the ICM is happening.

Extensive efforts have been made for the two limiting cases by previous analytical work. For an instantaneous outburst, it follows the classic ST solution at $t_{age}/t_E \rightarrow 0$ (Taylor 1946; Sedov 1959) while at $t_{age}/t_E \rightarrow \infty$ the shock wave driven by the outburst asymptotically approaches a sound wave due to the ambient pressure. The transition from classic ST solution to the asymptotic wave-like solution is studied by Mel'nikova (1954) and Sakurai (1954) according to perturbation theory but only valid when the deviation from ST solution is not very large. The asymptotical behavior of the outburst at $t_{age}/t_E \rightarrow \infty$ has been studied by Landau (1945) and Bethe et al. (1958) but focusing on the decay of the shock front. The global structure and energy partition of the outburst however are not discussed in detail. For a continuous outburst, the self-similar solution as an extension of the classic ST solution is available at $t_{age}/t_E \rightarrow 0$ (Dokuchaev 2002; Masuyama, Shigeyama, & Tsuboki 2016), if the energy injection in space and time satisfies certain conditions. At $t_{age}/t_E \rightarrow \infty$, the shock front gradually decays due to ambient pressure and eventually disappear. No wave-like structure is generated in a continuous outburst, because the energy injection never quenches and thus no rarefaction structure is formed behind the shock front.

The transition between the asymptotic ST solution at $t_{age}/t_E \rightarrow 0$ to the asymptotic wave-like solution at $t_{age}/t_E \rightarrow \infty$ is difficult to model analytically and will be studied numerically. The time evolution of an outburst with finite t_b hasn't been discussed before and will become the focus of this paper. Our final goal is to link the observables to all major characteristics of the outburst, including E_{inj} , t_b and t_{age} , and then differentiate between cases according to different t_b/t_E ratios. Among these observables the most easily accessible are: the Mach number M and the radius of the shock front R_s , and the radius of the ejecta R_{ej} . The latter quantity can be derived from observations by measuring the size of "radio bubbles" inflated by an AGN. We therefore investigate the relation between these observables and the characteristic properties of the outburst in detail for different combinations of E_{inj} , t_b and t_{age} . In section 3, we present the results for uniform ambient medium. Next, in section 4, we discuss how a more realistic radial profile of the ambient medium affects the results from uniform medium case. The numerical method used in this paper is described in Appendix D.

3 OUTBURST IN A UNIFORM MEDIUM

In this section, we investigate the dynamical evolution of an outburst in a uniform media with constant density and pressure profile, i.e. $\rho_a(r) = \rho_0$ and $P_a(r) = P_0$. We will focus on the spatial structure and energy distribution of the outburst during the transition from the ST phase to the wave-like phase. The natural way to illustrate the complete physical picture is to divide the problem into different regimes based on the t_b/t_E ratio and then investigate the physical properties of an outburst as a function of t_{age}/t_E in each individual regime closely. In this section, all the results are presented in dimensionless form to keep the generality of our discussion.

In order to demonstrate the energy distribution of an outburst over radius, we calculate cumulative kinetic E_{kin} and thermal E_{th} energies, which are defined as follows

$$E_{kin}(r, t_{age}) = \int_0^r \frac{1}{2} v^2(r', t_{age}) dM(r'), \quad (3)$$

where $v(r, t_{age})$ is the flow velocity at radius r and age t_{age} , and

$$E_{th}(r, t_{age}) = \int_0^r e(r', t_{age}) dM(r') - \int_0^r e(r', 0) dM(r'), \quad (4)$$

where $M(r')$ is the mass within radius r' and $e(r, 0)$ is the initial distribution of internal energy per unit mass in the ambient medium. In the calculation of E_{th} , we subtract the initial internal energy in the swept up materials to focus on only the spatial distribution of the injected outburst energy E_{inj} . Based on energy conservation $E_{th}(R_s, t) + E_{kin}(R_s, t) = E_{inj}$, where R_s is the radius of an outburst. When $t_{age}/t_E \gg 1$ (or equivalently $R_s(t_{age})/R_E \gg 1$), the initial thermal energy within R_s becomes much larger than the injected outburst energy, i.e. $\int_0^{R_s} e(r, 0) dM(r) \gg E_{inj}$. This limits the accuracy of evaluating E_{th} from eq. (4) in numerical simulations. Therefore, we constrain all the numerical runs to $t_{age} \leq 10t_E$ to ensure accurate determination of E_{th} .

We will start with a discussion about the two limiting cases, namely, the instantaneous outburst with $t_b/t_E \rightarrow 0$ and the continuous outburst with $t_b/t_E \rightarrow \infty$. A sketch of the spatial structure for both instantaneous and continuous outbursts at late time $t_{age} \gtrsim t_E$ is shown in Fig.1. Here late time refers to the stage that the shock front is moving much faster than the ejecta front, i.e., the shock has detached from the central ejecta bubble. In both cases, the affected volume could be divided into three different regions, ejecta (injected hot plasma), strongly shock-heated (SSH) and weakly shock-heated (WSH) gas envelopes, according to their composition and the entropy change during the evolution. In the continuous outburst, the amount of SSH gas is negligible. The physical properties of each region and the explanation of shock detachment process will be discussed in detail in the rest of this section.

3.1 Instantaneous outburst ($t_b/t_E \rightarrow 0$)

The transition from the ST phase to the wave-like phase for an instantaneous outburst has been examined in Tang & Wang (2005) (see also reference therein) in the context of a supernova explosion with a focus on the kinematics of the shock front. For AGN driven outburst in galaxy or

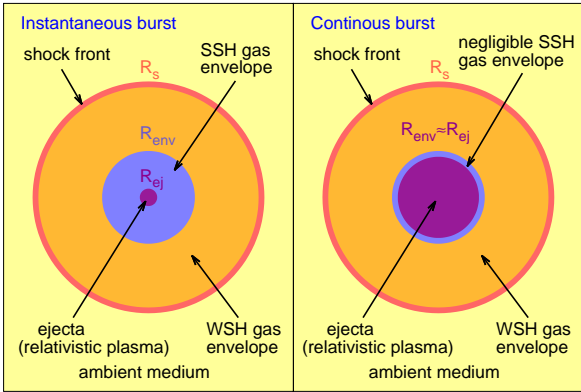


Figure 1. Sketch of the spatial structure of an outburst after the shock detachment (see also Forman et al., 2016). The left panel is for an instantaneous outburst and the right panel is for a continuous outburst. SSH and WSH stand for strongly shock heated and weakly shock heated regions, respectively. R_s is the shock front radius, R_{env} is the boundary that separates the SSH gas envelope from the WSH gas envelope, and R_{ej} is the ejecta radius.

cluster interested here, we instead concentrate on the spatial structure and energy distribution of the outburst.

As discussed by Tang & Wang (2005), after the ST phase the blast wave driven by the outburst gradually transforms from a strong shock to a weak shock since the internal energy in the swept up materials becomes dynamically important. In Fig. 2, we present the density ρ , temperature T , pressure P and velocity v profiles for an instantaneous outburst at different values of t_{age}/t_E to illustrate the development of two important features, namely, a shock detachment process and an emergence of a wave-like structure. As t_{age}/t_E increases, a weak shock front gradually detaches from the central bubble with high-temperature and low-density, which slows down with time and eventually becomes static. It is shown in Fig. 2 that, especially the panels for temperature and density profiles, the shock front is expanding away from the central hot bubble with time which implies the existence of a shock detachment process. After the shock detachment process, a wave-like structure with both crest and trough in the radial profile starts to emerge behind the shock front, which is more easily seen in the panels for pressure and velocity distribution. During the expansion, the shock velocity asymptotically approaches the speed of sound in the surrounding medium. See Appendix E for a simple analytical approximation of shock evolution in an instantaneous outburst, which is consistent with numerical simulation within a few percent accuracy.

As shown in Fig. 1, the spatial structure of an instantaneous outburst after shock detachment process could be divided into three different regions: ejecta, SSH and WSH gas envelopes (see, e.g., discussion in Xiang et al. 2009; Zhuravleva et al. 2016; Forman et al. 2017). In the left panel of Fig. 3, we plot the density ρ , cumulative thermal energy E_{th} and kinetic energy E_{kin} distributions of an instantaneous outburst at $t_{age}/t_E = 4$ for all three different regions.

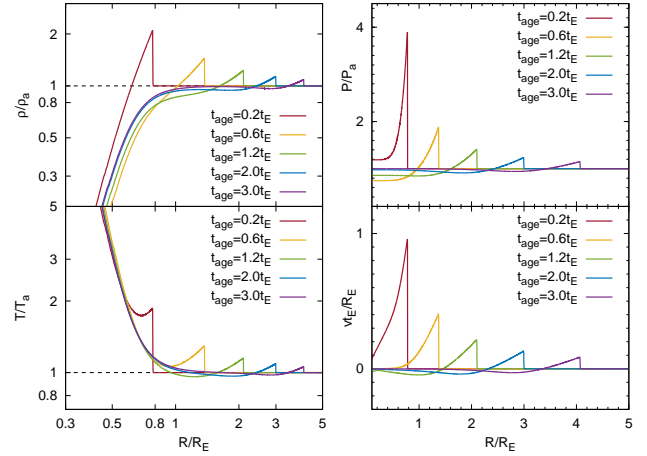


Figure 2. Radial profiles of ρ , T , P and v for an instantaneous outburst at different values of t_{age}/t_E . All quantities are normalized to the unperturbed values. The panels for density ρ and temperature T are in log scale while panels for pressure P and velocity v are in linear scale to emphasize various features emerging during the evolution. Dashed horizontal lines correspond to the unperturbed profiles.

The physical properties of the three regions are outlined below.

(1). Ejecta (hot plasma injected by an AGN). This is the innermost region with $r < R_{ej}$. It has the highest temperature (energy per unit mass) and the lowest density among all three different regions. For an instantaneous outburst, the thermal energy left in the ejecta after shock detachment is negligible as shown in Fig. 3. The kinetic energy of the ejecta is also negligible since at $t_{age} > t_E$ the pressure gradients in the injected hot plasma are quickly erased and the region becomes static. In observations, the relativistic particles in this region could produce synchrotron radio emission. In X-ray, it is revealed as a cavity/depression in the surface brightness due to the low density/emissivity.

(2). SSH envelope. This region corresponds to the gas that went through a strong shock and undergoes significant entropy increase. It starts at the outer boundary of ejecta R_{ej} and ends at R_{env} . R_{env} is defined as the radius where the entropy change of the shocked medium satisfies $S[r(t_{age}), t_{age}] - S[r(0), 0] = 0.1(\gamma_a - 1)c_v$. c_v is the heat capacity per unit mass. Note $r(t_{age})$ is in Lagrangian coordinate and the definition of R_{env} here is rather arbitrary. In the SSH region the gas properties gradually change from the hot and low density gas in the inner part to almost unperturbed values at R_{env} where SSH joins the WSH envelope, as shown in Fig. 3. No prominent synchrotron emission is expected from the SSH region, unless the strong shock leads to particle acceleration. For an instantaneous outburst, the size and amount of gas in this region is significant. So it might be detectable in X-ray observations as a hot and low surface brightness region, enveloping the ejecta. For a continuous outburst, the entropy increase is negligible; thus no SSH region is expected.

(3). WSH envelope. This region between R_{env} and R_s contains the gas that went through the shock, but the shock was too weak to induce significant entropy change in the

gas. The WSH region could be further subdivided into two parts based on their physical properties. Behind the shock front there is a wave-like structure (WLS) with both crest and trough along the radius. The WLS starts roughly at the position R_w where E_{th} starts to decrease with radius, i.e. the smallest radius satisfy $dE_{th}(r, t)/dr < 0$. Between R_{env} and R_w , the shocked medium has physical properties close to the unperturbed value. The two parts could be easily identified in the E_{th} distribution shown in Fig. 3. Between R_{env} and R_w the value of E_{th} increases very slowly, while between R_w and R_s , i.e. in the WLS region, E_{th} first drops steeply and then rise quickly with radius. The WLS moves at a speed asymptotically approaching the sound speed as $t_{age}/t_E \rightarrow \infty$ and carries almost all the kinetic energy induced by the outburst.

The late time evolution of an instantaneous outburst after the shock detachment is not discussed in detail in Tang & Wang (2005). Here we extend their analysis and show the behaviour of different energy components in all three regions after the shock detachment in the right panel of Fig. 3. The shock detachment time t_d is defined in the simulation as the time when a trough shape like structure emerges in E_{th} , i.e. the smallest time that satisfy $dE_{th}(r, t)/dr < 0$. For an instantaneous outburst, we find $t_d \approx 0.8t_E$ which corresponds to a Mach number $M \approx 1.25$ according to eq (E1) in Appendix E. After the shock detachment, the spatial structure and energy distribution in the ejecta and SSH gas envelope are essentially independent of time as shown in Fig. 2 and 3, respectively. At $t_{age}/t_E \gg 1$, the WLS structure carries all the kinetic energy of the system. E_{kin} asymptotically approaches a value $\lesssim 6\%$ of the injected outburst energy E_{inj} . As $t_{age}/t_E \rightarrow \infty$ the WLS becomes a sound wave, and it is expected that the total energy eventually carried away by the WLS would be $E_{th} + E_{kin} = 2E_{kin} \approx 12\%$. It provides an estimate of the amount of energy that will eventually leave the system with sound waves.

3.2 Slow piston driven outburst ($t_b/t_E \rightarrow \infty$)

In the previous section, the energy is released instantaneously and the ejecta are expanding supersonically which drive a strong shock into the ambient gas. We now consider an opposite limit, the so called ‘‘slow piston driven outburst’’, in which the ejecta expand very slowly. In this limit, the energy is assumed to be injected at a infinitely slow rate and the ejecta expand extremely slowly with negligible kinetic energy. Under such assumption, no strong shock is generated and no energy dissipation happens in the ICM during the expansion of ejecta. All the injected energy is transferred to the thermal energy of the ejecta and the PdV work, i.e. $E_{inj} = PV + PV/(\gamma_{ej} - 1) = \gamma_{ej}PV/(\gamma_{ej} - 1)$ where P and V are pressure and volume of the inflated ejecta bubble and γ_{ej} is the specific heat index of the injected plasma. For $\gamma_{ej} = 5/3$, the total energy, i.e. thermal energy, stored in the ejecta becomes $E_{ej} = E_{inj}/\gamma_{ej} = 0.6E_{inj}$ while the remaining $0.4E_{inj}$ is distributed over the swept up ambient medium.

This slow piston driven outburst is an idealized limit. A more plausible case to consider is when the energy is injected at a constant rate L . In this case, the ejecta initially expand supersonically, but with time the expansion velocity

of ejecta gradually becomes subsonic despite ongoing energy injection. Energy injected during the subsonic phase is accompanied by negligible dissipation at the shock front. As a result, while the total injected energy $E_{inj} = Lt_{age}$ increases linearly with time, the total energy dissipated during the outburst remains almost the same, making the percentage of various energy components in such a continuous outburst resemble the values in a slow piston limit. It is convenient to introduce a new set of characteristic time t_L and length R_L , similar to t_E and R_E , for a continuous outburst. Basically, in eqs. (1) and (2) one sets $E_{inj} = Lt_L$ and replaces R_E and t_E with R_L and t_L (see Appendix C for detail discussion). By definition, it is obvious that $t_L = t_E^{3/2}/t_b^{1/2}$. The time evolution of Mach number M for both an instantaneous outburst and a quasi-continuous outburst with $t_b = 10t_E$ is presented in Fig. E1. From this Figure, it is clear that the value of M drops below 0.1 at $t_{age} \sim 0.5t_E$ for the quasi-continuous outburst with $t_b = 10t_E$, which indicate the outburst has a very weak shock for almost 95% of the outburst duration t_b . As $t_b/t_E \rightarrow \infty$, the quasi-continuous outburst approaches a continuous outburst with no strong shocks being generated.

For a continuous outburst, after shock detachment its spatial structure mainly consists two regions, ejecta and WSH gas envelope, as shown in the right panel of Fig. 1. The SSH gas envelope now becomes negligible since the energy dissipation in a continuous outburst is negligible (only happening when $t_{age} \lesssim t_L$). In the left panel of Fig. 4, we plot the density ρ and accumulated thermal energy E_{th} distribution for a continuous outburst with $t_{age} = 2.82t_L$. The distribution of E_{kin} is not shown in this figure, as for a continuous outburst the kinetic energy is negligible after the shock detachment. The ejecta bubble in a continuous outburst has uniform density and temperature profiles which are different from those in an instantaneous outburst. The shock front driven by the outburst still asymptotically approaches the sound speed like in an instantaneous outburst. No WLS appears in the density and accumulated thermal energy distribution during the evolution as shown in Fig. 4. Instead E_{th} increases monotonically with radius in a continuous outburst which is also different from an instantaneous outburst. It is mainly because the energy injection in a continuous outburst hasn’t quenched before.

In the right panel of Fig. 4, we present the time evolution of different energy components in the two regions. The shock detachment process in a continuous outburst happens at $t_{age} \sim t_L$ according to the energy distribution of various components. As t_{age}/t_L increases, the amount of thermal energy stored in the ejecta quickly approaches the slow piston value, i.e. $E_{ej}/E_{inj}(t_{age}/t_E \rightarrow \infty) = 1/\gamma_{ej} = 60\%$ where $\gamma_{ej} = 5/3$, while the kinetic energy carried away by the WSH gas envelope quickly shrinks to almost zero. It is clear that all the energy components presented in the figure asymptotically approach the value in a slow piston driven outburst. Shock evolution in a continuous outburst is described in Appendix E with detail. A simple analytical approximation for shock evolution in a continuous outburst which is consistent with numerical simulation within a few percent accuracy is also provided in Appendix E.

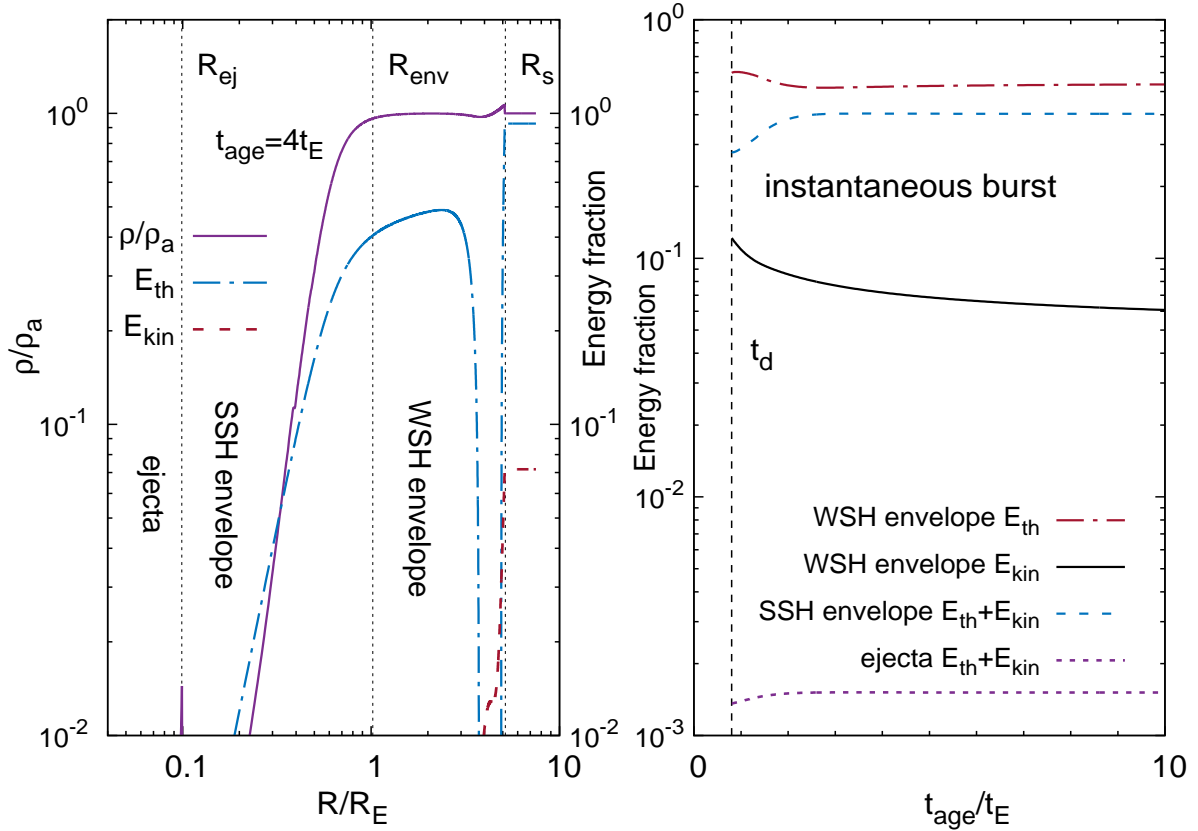


Figure 3. Left panel: Spatial structure of an instantaneous outburst at $t_{age} = 4t_E$. A large fraction of injected energy E_{inj} is stored in the SSH envelope while the energy left in the ejecta is negligible. A WLS with both crest and trough along the radius is presented in the density ρ distribution behind the shock front. The thermal energy E_{th} distribution shows a sharp decrease and subsequent increase in WLS. Right panel: Time evolution of various energy components from shock detachment $t_{age} = t_d \approx 0.8t_E$ to $t_{age} = 10t_E$. After the shock detachment, all energy components quickly approach the asymptotic values and then remain almost unchanged.

3.3 Intermediate regime

In the previous two subsections, we discussed the spatial structure and energy distribution of an instantaneous outburst ($t_b/t_E \rightarrow 0$) and a continuous outburst ($t_b/t_E \rightarrow \infty$). Now, we consider an intermediate case and study how the solution changes from a nearly instantaneous outburst to a nearly continuous outburst as t_b/t_E increases. The spatial structure and energy partition of an outburst in a uniform medium are mainly determined by two dimensionless ratios t_b/t_E and t_{age}/t_E , where t_E works like a scaling factor. As t_{age}/t_E increases, the time evolution of an outburst is characterized by the transition from a strong shock to a weak shock and eventually a sound wave (see discussion in section 2 and Appendix B).

In this section, we focus on the energy partition during such transition, especially the asymptotic behavior, for different t_b/t_E . For numerical purposes we take $t_{age} = 10t_E$ in lieu of the definition $t_{age} \rightarrow \infty$ and vary t_b/t_E from 0 to 10. At $t_{age} = 10t_E$ the shock is already very weak and further dissipation at the shock front should not change the energy partition significantly. The spatial structure of an outburst with different E_{inj} (related to t_E) and t_b at a fixed shock radius R_s is investigated in [Forman et al. \(2017\)](#) with the

density and temperature profile of M87. Despite the fact that medium in M87 is non-uniform, their results are consistent with our discussions here if proper t_E and R_E are chosen. Time evolution and energy partition of an outburst in a non-uniform medium will be discussed in detail in section 4.

A change in the t_b/t_E parameter causes strong rearrangements in the inner and outer parts of the affected volume. Here the inner part refers to the ejecta and SSH envelope while the outer part corresponds to WSH envelope including the WLS. We illustrate this in Fig. 5, which shows the logarithmic density profile of the inner part, while the inlay presents the density profile of the outer part in linear scale. Based on these plots we can introduce a characteristic value of $t_b/t_E \sim 0.5$ which separates the regime of “short/fast” outbursts from that of “long/slow” outbursts.

In the short/fast outburst regime ($t_b \lesssim 0.5t_E$), the outer part is weakly sensitive to t_b/t_E and resembles the outcome of an instantaneous outburst. In contrast, the structure of the inner part is very sensitive to the t_b/t_E ratio. As shown in Fig. 5, the size of the ejecta bubble and the energy stored in it increases very quickly with t_b/t_E . At the same time, the amount of gas in the SSH envelope and the energy stored within it decreases quickly with t_b/t_E , and becomes negli-

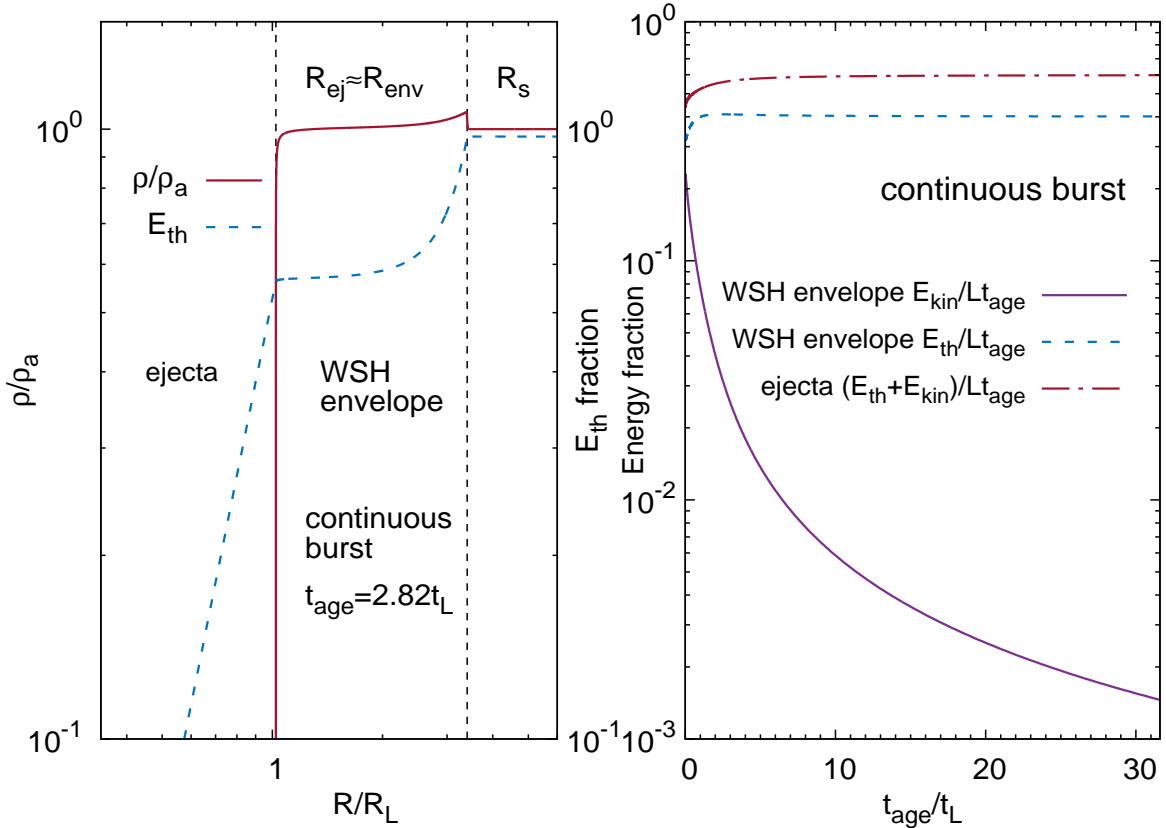


Figure 4. Left panel: Spatial density ρ and cumulative thermal energy E_{th} distribution for a continuous burst at $t_{age} = 2.82t_L$. SSH envelope becomes negligible now and close to 60% of injected energy E_{inj} is stored in the ejecta. No WLS appears in the density and cumulative thermal energy distribution. E_{th} now increases monotonically with radius. Right panel: Time evolution of different energy components in a continuous burst with constant energy injection rate L . All energy components approach the values in a slow piston driven outburst as t_{age}/t_L increases.

gible for $t_b/t_E \gtrsim 1$. Thus, the key signature of a short/fast outburst is the presence of a SSH envelope, i.e. hot and low density shell around the ejecta. We assume that observationally the ejecta can be identified as a boundary of the radio-bright region. The presence of the SSH envelope just outside ejecta could reveal itself in X-rays as a low surface brightness ring. To the best of our knowledge such structures have not been found in real objects.

In the slow/long outburst regime ($t_b/t_E \gtrsim 0.5$), the inner and outer parts respond to the change of t_b/t_E in a completely opposite way. While the inner region is insensitive to the value of t_b/t_E , the outer region changes considerably as shown in Fig. 5. As t_b/t_E increases, the Mach number of the shock front decreases and the amount of energy carried away by the WLS drops quickly with increasing t_b/t_E and eventually becomes negligible.

3.4 Energy partition in AGN driven outburst

For an AGN driven outburst in galaxy or cluster, we are particularly interested in the following question - what fraction of the injected outburst energy E_{inj} could escape from the system (i.e., escape to very large distances), and what

fraction could contribute to balancing the gas cooling loss in the cluster core? After the shock detachment, the ejecta and the shock heated gas envelope gradually slow down and their contribution to the kinetic energy becomes small. All the kinetic energy is instead associated with the outgoing (weak) shock and the gas behind it. As $t_{age}/t_E \rightarrow \infty$, the shock transforms into a sound wave and the value of E_{kin} approaches its asymptotic value. The energy carried away by the wave, which eventually escape from the system, would then simply be $E_{out} = 2E_{kin}$. The remaining part $E_{inj} - E_{out}$ is distributed in the ejecta and shocked materials. When $t_{age} \gg t_E$, all motions are already subsonic and no further dissipation is taking place. The amount of energy that ejecta and the swept up gas can release as radiation losses, when returning to its initial state, can be estimated as follows. Consider a gas shell with initial pressure $P_0 = P_a$ and volume V_0 . During the outburst, the pressure and volume of the shell becomes P_c and V_c respectively. Now imagine that at first the gas returns to its original pressure P_0 quickly enough, so that radiative cooling can be neglected. At this moment, the volume of the gas is $V_1 = V_c(P_c/P_0)^{1/\gamma}$, where γ is the specific heat index of the gas shell. The gas then radiatively cools and recovers the initial volume V_0

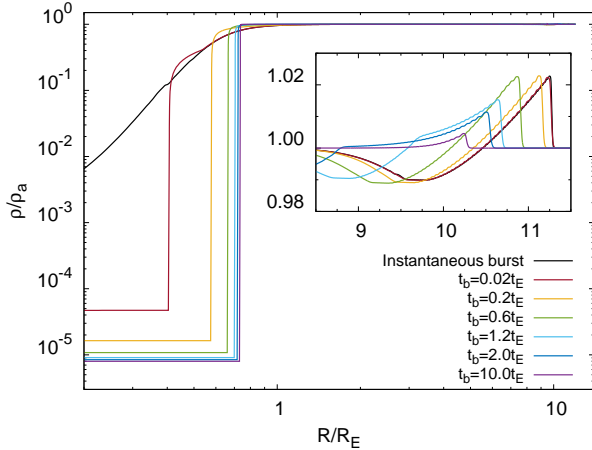


Figure 5. Normalized radial density profiles in logarithmic scale for an outburst at $t_{age} = 10t_E$ for different values of t_b/t_E , illustrating the transition from a “short/fast” outburst to a “long/slow” outburst. When $t_b/t_E \lesssim 0.5$, the structure of inner part has a strong dependence on the value of t_b/t_E while the outer part remains almost the same. The inset shows the same profiles in linear scale, but focusing on the outer part near the shock front. In contrast to the inner structure, the outer part is most sensitive to the values of $t_b/t_E \gtrsim 0.5$.

while maintaining the pressure equilibrium with the environment. The amount of energy released through radiative cooling is then

$$H = \frac{\gamma}{\gamma - 1} P_0 V_0 \left[\left(\frac{P_c}{P_0} \right)^{1/\gamma} \left(\frac{V_c}{V_0} \right) - 1 \right]. \quad (5)$$

We can now calculate the contributions to this energy from the swept up material H_{swept} and ejecta H_{ej} by integrating eq. (5) over their volumes at any moment of the simulations when the phase of shock heating is over.

For the swept up material, the value of H_{swept} characterizes the amount of ICM heating that has already happened during the shock propagation through the gas. In the case of a long or continuous outburst ($t_b \gg t_E$), the amount of shock heating is small comparing with E_{inj} at time $t_{age} \gg t_E$ and therefore $H_{swept} \ll E_{inj}$. In the opposite limit of an instantaneous outburst ($t_b \ll t_E$), H_{swept} is expected to be comparable to E_{inj} .

For ejecta, the initial volume V_0 is negligible. Therefore

$$H_{ej} \approx \frac{\gamma_{ej}}{\gamma_{ej} - 1} P_0 V_c \left(\frac{P_c}{P_0} \right)^{1/\gamma_{ej}}. \quad (6)$$

Furthermore, at $t_{age} \gg t_E$, the pressure in the entire central region relax to a value very close to the initial pressure P_0 , i.e., $P_c \approx P_0$. As a result, the above equation simply reduces to $H_{ej} \approx \frac{\gamma_{ej}}{\gamma_{ej} - 1} P_0 V_c$, i.e. enthalpy of the ejecta. Although this energy is associated with the ejecta and does not correspond to the ICM heating, it has been argued that if buoyant ejecta rise in the cluster atmosphere over several pressure scale-heights, then its enthalpy could be transferred to the ICM and used for ICM heating (e.g., Churazov et al. 2001, 2002; Begelman 2001). Unlike H_{swept} , the value of H_{ej} is expected to be large for a long outburst and small for a short outburst.

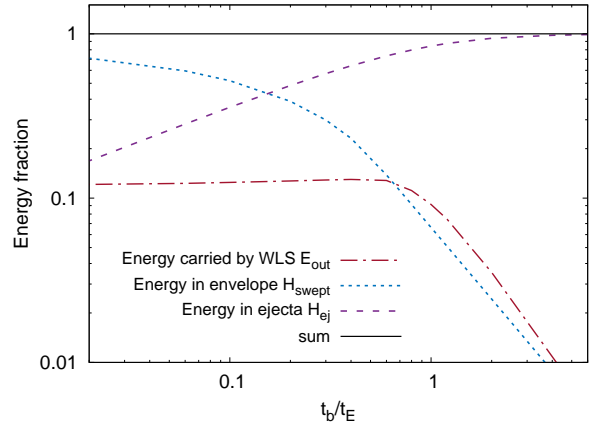


Figure 6. Dependence of energy partition among various components on the ratio t_b/t_E . The partition of energy is evaluated at $t_{age}/t_E = 10$ which could be considered as a good approximation for the asymptotic limit at $t_{age}/t_E \rightarrow \infty$. The small values of t_b/t_E correspond to a short outburst, with significant fractions of energy in all components. As t_b/t_E increases the limit of slow piston driven outburst is attained.

The above arguments are illustrated in Fig. 6, where we plot E_{out} , H_{swept} and H_{ej} evaluated at $t_{age} = 10t_E$ for different t_b/t_E . All values are normalized by the injected energy E_{inj} . The sum $(E_{out} + H_{swept} + H_{ej})/E_{inj}$ equals to unity and satisfies the condition of energy conservation, which indicates that our calculations are self-consistent. As shown in Fig. 6, when $t_b/t_E < 0.5$, the ratio $E_{out}/E_{inj} \approx 0.12$ remains constant and is consistent with the value for an instantaneous outburst. When $t_b/t_E > 0.5$, the amount of escaping energy drops very quickly as t_b/t_E increases. When $t_b/t_E > 4$, the amount of energy that could escape from the system already drops below 1% of E_{inj} and the evolution of the outburst becomes close to a slow piston driven/continuous outburst. The contribution of H_{swept} to the total energy is expected to be maximal for an instantaneous outburst, in which the contribution of H_{ej} is negligible. The asymptotic value $H_{swept} \sim 0.88E_{inj}$ corresponds to a very short outburst (beyond the minimal value of t_b/t_E shown in the plot). As t_b/t_E increases the value of H_{swept} drops and becomes less than 10% at $t_b/t_E \sim 1$. On the contrary, H_{ej} steadily increasing with t_b/t_E ; it exceeds 50% at $t_b/t_E \sim 0.2$ and approaches unity for very long outbursts. For the continuous outburst model in stratified atmospheres of clusters, buoyancy forces break the bubble and displace it when the expansion of the ejecta becomes substantially subsonic (e.g., Churazov et al. 2000). This corresponds to large values of t_b/t_E . It is therefore likely that in clusters the main repository of released energy is the enthalpy of the ejecta H_{ej} .

According to eq. (6), it is clear that the amount of energy stored in the ejecta is determined by the size (volume) of the ejecta. In X-ray observation, the ejecta can be identified as a radio-bright and X-ray-dim region. The dimensionless ratio of the shock radius R_s and the ejecta radius R_{ej} then becomes an important physical quantity characterizing the properties of the outburst. This quantity is also

easy to evaluate from observations, apart from the uncertainty caused by the deviations from spherical symmetry. For a continuous outburst, an analytical approximation for the R_s/R_{ej} ratio is available, which is presented in Appendix E.

4 NON-UNIFORM MEDIUM

In this section, we use the Perseus cluster and M87 as examples to show that the dynamical evolution of an outburst in a monotonous, smooth and shallow (power index $\lesssim 2$) density and pressure profiles is qualitatively similar to that in a uniform medium. Moreover, we show below that for the same characteristic length R_E and time t_E , the quantitative predictions of an outburst in uniform medium reproduce major variables with an accuracy of 20-30 per cent. It enables us to develop simple tools, based on the simulations in a uniform medium, to estimate intrinsic properties of an outburst in a non-uniform medium without running numerical simulation tailored to each specific case.

In a uniform medium, the characteristic length and time scales are defined by eqs. (1) and (2). For a more realistic case, when $P_a(r)$ and $\rho_a(r)$ vary with radius, it is natural to replace eq. (1) that defines R_E with

$$E_{inj} = \int_0^{R_E} P_a(r) 4\pi r^2 dr. \quad (7)$$

For the time scale t_E , one could replace the sound speed c_s in eq (2) with volume averaged value, i.e. adopt the volume averaged temperature \bar{T} to calculate c_s . R_E and t_E defined with the above method could be used to characterize the evolution of an outburst in a non-uniform medium. But for the galaxies and clusters of interest here with shallow density and pressure profiles, a simpler definition of R_E and t_E with pressure and density at the shock front, i.e.

$$E_{inj} = \frac{4\pi}{3} P_a(R_s) R_E^3, \quad (8)$$

and

$$t_E = \frac{R_E}{\sqrt{\gamma_a P_a(R_s)/\rho_a(R_s)}}, \quad (9)$$

are found to provide results close to those derived with volume averaged quantities. In the rest of discussion, unless specifically noted we will use the definitions in eq (8) and (9) for simplification.

The primary goal of this section is to develop simple tools to map major observables to intrinsic properties of an outburst, which could be easily applied to different objects. Before we present the tools developed according to simulation in a uniform medium, we run simulations for outbursts in realistic cluster profiles of $P_a(r)$ and $\rho_a(r)$ taken from observations and verify that the predictions of uniform medium runs agree with more accurate calculations.

4.1 Numerical Simulations for M87 and the Perseus cluster

The observed values of shock radius R_s , ejecta radius R_{ej} and Mach number M for these two objects are listed in Table 1. The volume averaged pressure \bar{P} and density $\bar{\rho}$ within the

Table 1. Basic parameters of M87 and Perseus cluster from observation

object	M87	Perseus cluster
R_s (kpc)	13.0	15.0
R_{ej} (kpc)	3.0	7.5
M^a	1.2	1.16
$\bar{\rho}^b$ (cm $^{-3}$)	4.5×10^{-2}	0.1
\bar{P}^b (keVcm $^{-3}$)	7.8×10^{-2}	0.35
n_s^c (cm $^{-3}$)	3.1×10^{-2}	0.1
P_s^c (keVcm $^{-3}$)	5.6×10^{-2}	0.33
n_{ej}^d (cm $^{-3}$)	0.13	0.11
P_{ej}^d (keVcm $^{-3}$)	0.2	0.36
Reference	1,3,4,6	2,5

^a Assuming $\gamma = 5/3$.

^b Volume averaged quantities.

^c Quantities at the shock front R_s .

^d Quantities at the ejecta front R_{ej} .

1. Forman et al. (2007);
2. Graham et al. (2008);
3. Xiang et al. (2009);
4. Simionescu et al. (2009);
5. Zhuravleva et al. (2016);
6. Forman et al. (2017)

outburst in Table 1 are calculated with the ‘‘unperturbed’’ profiles presented in Appendix F.

For M87 and the Perseus cluster, we run a set of numerical simulations to search for a set of parameters (E_{inj}, t_b, t_{age}) which can reproduce the observed values (R_s, R_{ej}, M). Plausible sets of parameters (E_{inj}, t_b, t_{age}) derived from these simulations are summarized in Table 2 (see Appendix F for details). These values are consistent with previous works (Forman et al. 2007, 2017; Zhuravleva et al. 2016).

Based on these simulations, we concluded that the physical properties of an outburst in a non-uniform medium is qualitatively similar to that in a uniform medium (See Appendix F for details). The spatial structure of the outburst still contains three regions: ejecta, SSH and WSH as shown in Fig 1. The quantitative difference is mainly caused by two reasons. At first, t_E and R_E are evolving with time t_{age} for an outburst in a non-uniform medium. In a realistic galaxy or cluster profile like M87 and the Perseus cluster, t_E is increasing with time. As a result, t_b/t_E is decreasing with t_{age} and the outburst will appear to be a shorter/faster outburst as t_{age} increases. Secondly, gravity plays a role in the energy partition of an outburst. The shocked materials pushed by the central ejecta end up with a higher gravitational potential during the outburst. Therefore the amount of energy that could contribute to radiative cooling is not only determined by the enthalpy of the ejecta and shocked materials but also related to the gravitational energy of the shocked materials (gravitational energy of ejecta is negligible due to negligible mass). The energy carried away by the WLS however is not affected significantly by the non uniform environment with shallow profiles.

4.2 Simple tools based on simulation in uniform medium

In this subsection, we discuss simple recipes to estimate the intrinsic properties (E_{inj}, t_b, t_{age}) of an outburst based on observables (R_s, R_{ej}, M) in addition to ambient density $\rho(r)$ and pressure $P(r)$ profiles without running numerical simulation.

The age of an outburst t_{age} satisfies

$$t_{age} = \int_0^{R_s} \frac{dr}{M(r)c_s(r)} \quad (10)$$

where $c_s(r)$ is the sound speed at radius r and $M(r)$ is the Mach number of the outburst when its shock front arrives at the radius r . For outbursts in clusters or galaxies with shallow density and pressure profiles, the Mach number $M(r)$ is decreasing with radius r and time t_{age} during the evolution. Thus the dominant contribution to the above integral comes from the stage with $r \sim R_s$ and $M \sim M(R_s)$. Therefore we further assume

$$t_{age} = \frac{\chi R_s}{M(R_s)c_s(R_s)} \quad (11)$$

where $\chi \sim O(1)$ is a coefficient that depends on the evolution history of an outburst. As $t_{age}/t_E \rightarrow \infty$, the shock front becomes weak with $M \rightarrow 1$ and in the meantime χ asymptotically approaches the value of unity. According to above discussion, for outbursts with weak shock a simple estimate for t_{age} would be $t_{age} = R_s/M(R_s)c_s(R_s)$ as χ is expected to be close to 1 in such a situation.

In Fig. 7, we plot χ as a function of $M - 1$ for outbursts with different t_b/t_E in both uniform media and realistic galaxy profiles. It is found that, for a given Mach number, χ in a slower outburst is more close to 1. It is not a surprise, as shock in a slow outburst is weaker at early time. Besides χ derived from a non-uniform medium is larger than that from a uniform medium. It is mainly because Mach number in a realistic galaxy or cluster profile drops more slowly with time due to the density gradient. As a result, the outbursts spend more time in the small M regime, making χ closer to 1. For slow outbursts with weak shocks $M \lesssim 1.5$, it is found that χ is close to 1 with only about 20%–30% offset as shown in Fig. 7. So we could simply apply eq (11), assuming $\chi = 1$, to estimate t_{age} . More accurate t_{age} can be obtained if we use for example the continuous outburst line (blue solid) to correct χ for a slow outburst ($t_b/t_E \geq 0.5$) and the instantaneous outburst line (red solid) to correct χ for a fast outburst ($t_b/t_E < 0.5$). For M87 and the Perseus cluster, t_{age} estimated with eq (11) are presented in Table 2 and are consistent with numerical simulation results with 20%–30% accuracy.

Next let us discuss a possible way to derive t_b and E_{inj} based on available observables including shock radius R_s , ejecta radius R_{ej} , Mach number M and the pressure profile $P(r)$. To facilitate the comparison between observables and the intrinsic properties of an outburst, we apply two dimensionless numbers M and G to characterize the state of the system at a given time t_{age} . The first parameter M is simply the Mach number of the shock and the second parameter

$$G = \frac{P_s R_s^3}{P_{ej} R_{ej}^3}, \quad (12)$$

is the ratio of thermal energies within the volumes defined by the shock and ejecta radii, R_s and R_{ej} , respectively. Note in the above equation we replace the integration of the energy density over volume with the product of the volume and the pressure at the corresponding radius to further simplify the comparison. We then run a group of simulations in a uniform medium with different values of t_b/t_E . According to the simulation results, we further build map between (M, G) and

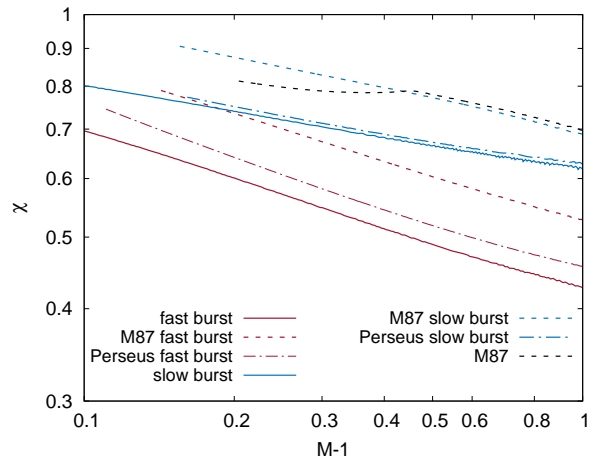


Figure 7. χ as a function of $M - 1$. χ is defined in eq (11) and could be considered as the ratio between simulated t_{age} and the estimation from simple analytical formula $t_{age} = R_s/M(R_s)c_s(R_s)$. $M(R_s)$ and $c_s(R_s)$ are the Mach number and sound speed at shock radius R_s . Solid, dashed and dotted-dashed lines are for simulation results in uniform medium, realistic profiles in M87 and realistic profiles in Perseus cluster respectively. Red lines are for fast instantaneous outburst while blue lines are for slow continuous outburst. For fast burst in M87 and Perseus cluster, we assume $E_{inj} = 5.5 \times 10^{57} \text{ erg}$ and $1.1 \times 10^{59} \text{ erg}$ respectively according to our best fit model. Black line is an intermediate outburst which represents our best fit model for M87. Blue dotted dashed line shows our best fit model for Perseus cluster. In the calculation of blue dashed line we apply $L \approx 7 \times 10^{43} \text{ erg s}^{-1}$ which is comparable with L from our best fit model for M87.

dimensionless ratios t_b/t_{age} and $E_{inj}/P_s R_s^3$, which could be used to calculate t_b and E_{inj} easily. In Fig. 8, we present the contours of $t_b/t_{age}(M, G)$ (left panel) and $E_{inj}/P_s R_s^3(M, G)$ (right panel) as a function of $M - 1$ and G . The bottom red solid line corresponds to a continuous outburst, while the top red solid line corresponds to a short outburst with $t_b/t_E = 2 \times 10^{-3}$. During the evolution of an outburst, the Mach number M decreases with t_{age} , so in Figs. 8 time increases from right to left. As long as $t_{age} \leq t_b$ the time evolution of an outburst follows the continuous outburst line. Once the outburst quenches, it gradually switches to a regime in which the shock radius linearly increases with time and the ejecta radius remains almost static.

Next we apply the map shown in Fig. 8 to estimate t_b and E_{inj} for M87 and the Perseus cluster based on observables presented in Table 1. The results are shown in Table 2 under the name of the mapping method. E_{inj} , t_b and t_{age} derived from our simple mapping method are found to be consistent with numerical simulations tailored for M87 and the Perseus cluster with a 20%–30% accuracy. The estimate for the Perseus cluster is better than M87, because the outburst in Perseus cluster is still in the core region with flat density and pressure profiles. As long as the density and pressure distribution in an outburst are not very steep (with power law index $\lesssim 2$), the mapping method discussed above according to simulation in a uniform medium should be able to provide a good estimate for E_{inj} , t_b and t_{age} . The validity

of the map shown in Fig. 8 is illustrated in Appendix G in detail.

Another way to estimate t_b and E_{inj} based on known t_{age} is to use Fig. 6 which can be used as an independent check for the mapping method. It requires a bit more calculation. In order to derive E_{inj} , we further introduce two physical variables,

$$E_c = \frac{4\pi R_{ej}^3 P(R_{ej})}{3(\gamma_{ej} - 1)} \quad (13)$$

and

$$E_a = (M - 1)^2 \frac{4\pi(R_s^3 - R_{ej}^3)P(R_s)}{3(\gamma_a - 1)}, \quad (14)$$

where R_{ej} and R_s are the ejecta and shock radius respectively. E_c is a approximation for the thermal energy stored in the ejecta bubble while E_a characterizes the thermal energy transferred into the shocked ambient medium.

For a continuous outburst, the injected energy $E_{inj} \approx \gamma_{ej} E_{ej} \approx \gamma_{ej} E_c$ according to the discussion in section 3. For a very short outburst, the bulk of the injected energy E_{inj} is transferred to the shocked ambient medium. We instead find $2\gamma_a E_a$ provides a good approximation of E_{inj} for the age range $(0.1t_E, 2t_E)$ we're interested in here. By combining the expressions for E_{inj} from the above two limiting cases, we end up with the following simple formula

$$E_{inj} = \begin{cases} \gamma_{ej} E_c + \gamma_a E_a, & \text{if } E_c \geq E_a \\ 2\gamma_a E_a, & \text{if } E_c < E_a \end{cases} \quad (15)$$

to estimate E_{inj} . Once we obtain E_{inj} , we can further derive t_b/t_E by comparing $\gamma_{ej} E_c/E_{inj}$ with the purple dashed line in Fig. 6 which represent the percentages of $\gamma_{ej} E_{ej}$. By using eq (9) to derive t_E , we can then calculate t_b easily. t_b and E_{inj} derived with this method are presented in Table 2 under the name of the analytical estimate. The results from analytical estimates are consistent with the mapping method and numerical simulations for both M87 and the Perseus cluster. In the calculation of t_b for the Perseus cluster, we found $t_b > t_{age}$ which is not physical. It is mainly because the results shown in Fig. 6 are intended for asymptotic values of the energy partition. The observed outbursts however may not have relaxed to such asymptotic values yet. As a result, we obtain an unreasonably large t_b . In such a situation, we simply assume $t_b = t_{age}$.

Note both the mapping method and the analytical estimate described in this section are designed for the late time evolution of an outburst when the shock front already detaches from the ejecta bubble and becomes a weak shock. Both the Perseus cluster and M87 are found to satisfy this condition. It is probably a selection bias, as outbursts at earlier times shall have smaller sizes which would be harder to resolve in observations. The dynamics of an outburst in early time will have stronger dependence on the asymmetry of the central AGN which is probably beyond the simple model discussed here.

5 CLASSIFICATION OF OUTBURSTS BY DURATION AND AGE

In the previous sections, we have already shown that the intrinsic properties of an outburst, i.e. t_b , t_E and t_{age} , can

be derived from major observables, i.e. R_s , R_{ej} and M plus density and pressure profiles of the galaxy or cluster. Here we demonstrate the classification of outbursts in a two-dimensional plot according to their physical properties (see Fig. 9). The horizontal axis is the dimensionless ratio t_{age}/t_E which characterizes the time evolution of an outburst. As t_{age}/t_E increases, the shock front in an outburst gradually transitions from a strong shock to a weak shock. The vertical axis is the dimensionless ratio t_b/t_E , which is mainly determined by the energy injection history of an outburst. As t_b/t_E increases, a short/fast outburst gradually changes into a long/slow outburst. In Fig. 9, t_{age} is simply the time elapsed since the onset of an outburst. The definition of t_b and t_E in this plot however requires extra explanation that is given below. In observations of a realistic object, it either quenched at past with $t_b < t_{age}$ or has ongoing energy injection with $t_b = t_{age}$. So in Fig. 9, we are only interested in the region with $t_b \leq t_{age}$. The black solid line from bottom left to top right represents the evolution track of an ongoing outburst. The characteristic time t_E is determined by the energy released since the onset of the outburst till t_{age} . Therefore, for a constant energy injection rate L , $E_{inj} = L \times \min(t_{age}, t_b)$, which implies t_E increases with time t_{age} before the outburst quenches. According to the above definitions, the time evolution of an outburst with $t_b/t_E = 0.1$ and $t_{age}/t_E = 1$ (black square in Fig. 9) would first proceed along the line $t_{age} = t_b$ until $t_{age} = t_b = 0.1t_E$ and then follow the horizontal black arrow with $t_b = 0.1t_E$ until $t_{age} = 1t_E$ to arrive at its current position in the plot.

Next we discuss the various regions presented in Fig. 9 to demonstrate various processes happening during the outburst. The dashed blue (almost vertical) line in Fig. 9 is the Mach number $M = 1.5$ line which is considered as an indicator for the transition between strong shock and weak shock. The blue solid vertical line schematically shows the region (to the right from this line) where in real clusters buoyancy effects become important. The value of t_{age}/t_E corresponding to this line is only indicative, since it depends on the interplay between the buoyancy and expansion velocity of the bubbles (e.g., Churazov et al. 2000). The main characteristic of this regime is that the expansion velocities of ejecta become substantially subsonic. The two red horizontal lines define three regions along t_b/t_E . Below the lower dashed line (very short outburst), the shock-heating is very significant and a prominent SSH gas envelope is formed and possibly detected in observations. Above the upper dotted-dashed line (very long outburst), the WLS is less significant and the energy carried away by the WLS already drops to a value below about 1% of E_{inj} . In real clusters this region is likely inaccessible since the buoyancy forces will disrupt the bubble before the outburst can evolve to this stage. In the region between the two red lines, shock heating is not important, but the WLS is still present.

We mark the approximate locus of M87 (triangle) and the Perseus cluster (circle) outbursts in this plot based on our best fit numerical simulation model shown in Table 2. Along the t_{age}/t_E axis, both observed outbursts are located in the region with $0.3 \lesssim t_{age}/t_E \lesssim 2$. It is not surprising, since selection effects make it difficult to detect an outburst in the early state with small t_{age}/t_E . Detection of outbursts in the very late stage ($t_{age}/t_E \gg 1$) is also unlikely as the buoyancy effects start to become important with time and

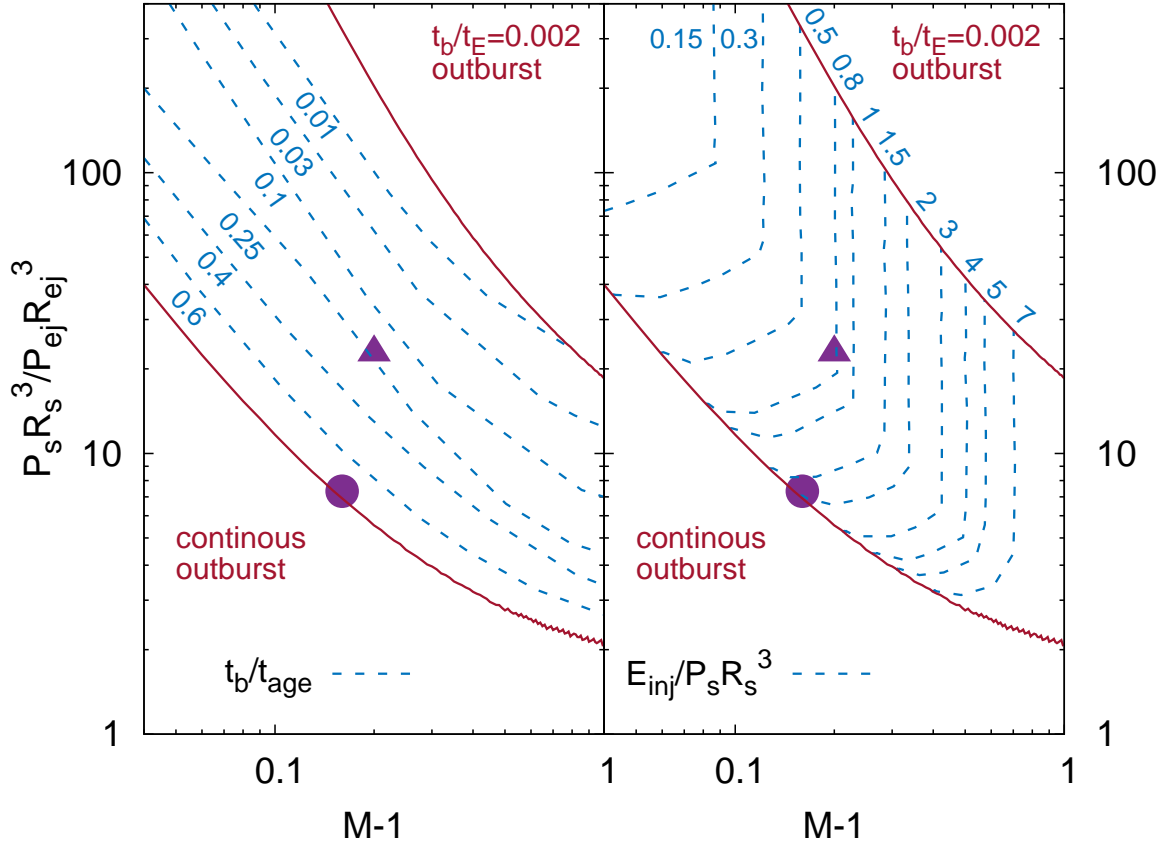


Figure 8. x axis: $M - 1$ where M is the Mach number of the shock wave; y axis: $P_s R_s^3 / P_{ej} R_{ej}^3$ where R_s is shock radius, R_{ej} is ejecta radius, P_{ej} is the pressure at R_{ej} and P_s is the pressure at R_s . Left panel: Red solid lines from top to bottom represent a fast outburst with $t_b/t_E = 0.002$ and a continuous outburst respectively. Blue dashed lines is the contour with different t_b/t_{age} ratios. Note the red continuous outburst line also indicates the line with $t_b/t_{age} = 1$. Right panel: Red solid lines from top to bottom again represent a fast outburst with $t_b/t_E = 0.002$ and a continuous outburst, respectively. Blue dashed lines show the contour with different $E_{inj}/P_s R_s^3$ ratios where E_{inj} is the total injected outburst energy. Purple triangle and circle are for M87 and Perseus cluster respectively based on numerical simulation results in Table 2. The size of the symbol is not a indication for the error bar.

Table 2. Basic parameters of M87 and Perseus cluster from different methods by fitting the outburst parameters in Table 1.

Object	Method	$E_{inj}(10^{58}\text{erg})$	$t_b(\text{Myr})$	$t_{age}(\text{Myr})$	$E_{inj}/P_s R_s^3$	t_b/t_E	t_b/t_{age}
M87	Numerical simulation	0.55	2.0	12.3	0.95	0.18	0.16
	Mapping method	0.46	3.3(2.4)	15(11)	~ 0.8	0.29(0.21)	~ 0.22
	Analytical estimate	0.5	2.8	15(11)	0.86	~ 0.25	0.18(0.24)
Perseus cluster	Numerical simulation	10.8	10.3	10.3	2.1	0.83	1
	Mapping method	9.3	11.7(9)	13(10)	~ 1.8	0.94(0.73)	~ 0.9
	Analytical estimate	8.9	11.8	13(10)	1.7	~ 0.95	0.9(1)

For simplicity, t_E is calculated with pressure P and density ρ at the shock front R_s .

Quantities in brackets are estimated with $\chi = 0.75$ based on the continuous outburst line in Fig. 7, while quantities outside the brackets are calculated with $\chi = 1$.

Note for analytical method there is conflict between t_b and t_{age} in Perseus cluster, see text for detail.

" \sim " symbol indicates quantities read from figures.

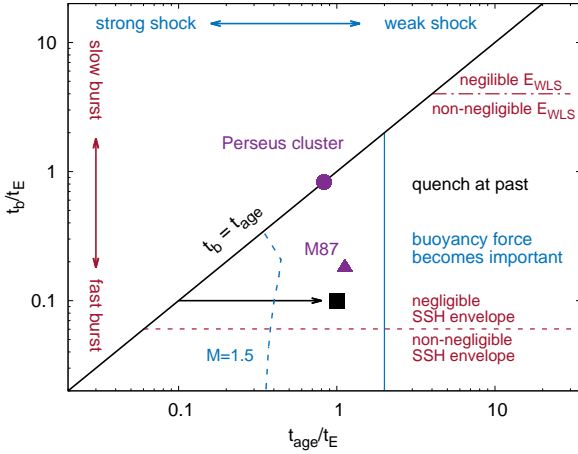


Figure 9. Schematic figure for outbursts in galaxy or cluster. Horizontal axis is the t_{age}/t_E ratio which indicates the time evolution. Vertical axis is the t_b/t_E ratio which represents the transition from fast outburst to short outburst. The black solid line from bottom left to top right shows the evolution track of an continuous outburst, i.e. $t_{age} = t_b$. The dashed blue (almost vertical) line shows the position with Mach number $M = 1.5$, which characterizes the transition from strong shock to weak shock (left to right). The blue solid vertical line schematically shows the region where in real clusters buoyancy effects become important (to the right from this line). The red dashed line separates the region with negligible SSH envelope and the region with non-negligible SSH envelope. Above the red dotted-dashed line, the energy carried out by the WLS structure already drops below 1% of E_{inj} and becomes negligible. Purple circle and triangle show the position for Perseus cluster and M87 respectively according to simulation results. Black square is an outburst with $t_b/t_E = 0.1$ and $t_{age}/t_E = 1$. The black arrow next to it indicates the time evolution of the outburst after it quenches at $t_b = 0.1t_E$.

can remove the ejecta (bubble) from the core region. The observed R_s , R_{ej} and M for the Perseus cluster suggest an ongoing outburst while the observed parameters for M87 imply its outburst has quenched long ago. These results are in line with previous findings (e.g., Forman et al. 2007, 2017; Zhuravleva et al. 2016). Along the t_b/t_E axis both outbursts fall into the range where shock heating is not very important and a small fraction of energy $\lesssim 12\% E_{inj}$ is carried by the sound wave. Most of the energy released in the outburst is captured by the enthalpy of the ejecta/bubble.

So far we have placed only 2 objects in this plot. In the future, with enlarged samples of objects we could possibly extract information on the duty cycle of the outbursts in galaxies and clusters by studying their distribution in the t_b/t_E v.s. t_{age}/t_E plot.

6 CONCLUSIONS

We have considered the evolution of a spherically symmetric outburst in a uniform medium with non-negligible pressure, having in mind AGN feedback in the intra-cluster medium (ICM). We, in particular, focused on the spatial structure and energy partition of the outburst during the transition from an early ST phase to a late wave-like phase.

The physical properties of an outburst in a homogeneous medium with pressure P_a and density ρ_a at age t_{age} are mainly determined by two quantities, the total injected energy E_{inj} and the duration t_b . E_{inj} , P_a and ρ_a together define the characteristic length scale R_E and time scale t_E of the system, as given by eqs. (1) and (2) respectively. The ratio t_b/t_E characterizes the energy injection history of the outburst. As the t_b/t_E ratio increases, the system changes from an instantaneous outburst with $t_b/t_E \ll 1$ to a continuous one with $t_b/t_E \gg 1$. In the former case, much of the energy ($\sim 88\%$) goes into the shock heated gas (at $t_{age}/t_E \gg 1$), while a small fraction of energy $\lesssim 12\%$ is carried away by the sound waves. The enthalpy of the ejecta is negligible. In the latter case, essentially 100% of energy is stored as the enthalpy of very hot ejecta, while the amount of energy spent on shock heating of the ambient medium or outgoing sound waves is negligible.

The enthalpy of the bubble, i.e. $H_{ej} \approx \frac{\gamma_{ej}}{\gamma_{ej}-1} P_0 V_c$ (Churazov et al. 2002), is usually adopted by observers to estimate the injection energy of an outburst E_{inj} . Based on discussion in 3.4, the ratio H_{ej}/E_{inj} varies from zero to one as t_b/t_E changes from zero to infinity. It is found that the outbursts in M87 (Virgo) and Perseus cluster have $t_b/t_E \approx 0.2$ and 0.8 respectively. According to Fig. 6, if we assume $\gamma_{ej} = 4/3$, $E_{inj}/P_0 V_c$ varies from 5 to 13 as t_b/t_E decreases from 1 to 0.1, which is consistent with the results in Birzan et al. (2004).

For the mechanical AGN feedback in cluster cores, the latter case ($t_b/t_E \gg 1$) seems to be more relevant. Indeed, under assumption of quasi-continuous energy release, the life-time of the bubbles is set by the competition of the buoyancy and the expansion of ejecta due to energy release (e.g., Churazov et al. 2000). Since this balance is achieved when velocities are substantially subsonic, this corresponds to $t_b/t_E \gtrsim 2$, where the enthalpy of the ejecta captures the dominant fraction of the energy.

We further show that for a spherically symmetric outburst the maximum amount of energy that is eventually carried away by a sound wave does not exceed $\sim 12\%$. This value is an upper limit, since we have neglected effects of conduction or viscosity that may further attenuate outward-going sound waves (e.g., Graham et al. 2008). We will study these effects in future work. Note that, for outbursts/outflows with strong anisotropy, the fraction of energy that goes into sound waves can be larger.

We also develop two simple methods to connect the observable (R_{ej} , R_s , M) to the intrinsic properties of an outburst (E_{inj} , t_b , t_E) based on the simulations of an outburst in a uniform medium. We then tested the accuracy of these approaches using numerical simulations incorporating realistic radial density and temperature profiles in M87/Virgo and the Perseus cluster. It is found that energetic outbursts in galaxies or clusters with a shallow profile (power law index $\lesssim 2$) are qualitatively similar to those in a uniform medium. The quantitative difference is also not very significant. Our approach recovers the values of (E_{inj} , t_b , t_E) from simulations tailored for these objects with 20% – 30% accuracy.

The main limitation of the above approach is the assumption of spherical symmetry. One can expect this approach to work reasonably well for energy-driven outflows, while for momentum-dominated jets the spherical symme-

try may be seriously violated. The diffuse morphology of typical Fanaroff-Riley type I radio sources in many cluster cores suggests that the energy-driven outflow is a reasonable assumption and therefore our conclusions hold at least approximately.

ACKNOWLEDGMENTS

We are grateful to the anonymous referee for useful comments which help to clarify some points in the manuscript. We would like to thank Roger Chevalier for many useful comments, which helped us to improve the manuscript. We're also grateful to Rashid Sunyaev and William Forman for useful discussions and collaborations on related projects.

REFERENCES

- Begelman M. C., 2001, ASPC, 250, 443
- Bethe, H. A., Fuchs, K., Hirschfelder, J. O., Magee, J. L., Neumann, R. V., 1958, Blast Wave (No. LA-2000), Los Alamos National Lab NM
- Birzan, L., Rafferty, D. A., McNamara, B. R., Wise, M. W., & Nulsen, P. E. J. 2004, ApJ, 607, 800
- Caramana, E. J., Shashkov, M. J., & Whalen, P. P. 1998, Journal of Computational Physics, 144, 70
- Chugai, N. N., Churazov, E. M., & Sunyaev, R. A. 2011, MNRAS, 414, 879
- Churazov E., Forman W., Jones C., Böhringer H., 2000, A&A, 356, 788
- Churazov E., Brüggem M., Kaiser C. R., Böhringer H., Forman W., 2001, ApJ, 554, 261
- Churazov E., Sunyaev R., Forman W., Böhringer H., 2002, MNRAS, 332, 729
- Churazov, E., Forman, W., Jones, C., & Böhringer, H. 2003, ApJ, 590, 225
- Dokuchaev, V. I. 2002, A&A, 395, 1023
- Fabian A. C., Sanders J. S., Taylor G. B., Allen S. W., Crawford C. S., Johnstone R. M., Iwasawa K., 2006, MNRAS, 366, 417
- Fabian A. C., 2012, ARA&A, 50, 455
- Forman, W., Jones, C., Churazov, E., et al. 2007, ApJ, 665, 1057
- Forman, W., Churazov, E., Jones, C., et al. 2017, arXiv:1705.01104
- Graham, J., Fabian, A. C., & Sanders, J. S. 2008, MNRAS, 386, 278
- Heinz S., Reynolds C. S., Begelman M. C., 1998, ApJ, 501, 126
- Hillel S., Soker N., 2016, MNRAS, 455, 2139
- Landau, L.D., 1945, Appl. Math. Mech., 9, 286
- Masuyama M., Shigeyama T., Tsuboki Y., 2016, PASJ, 68, 22
- McNamara B. R., et al., 2000, ApJ, 534, L135
- Mel'nikova, N. S., 1954, Zh. Mekhanika 3,2535
- Randall S. W., et al., 2011, ApJ, 726, 86
- Richtmyer, R. D., & Morton, K. W. 1967, Interscience Tracts in Pure and Applied Mathematics, New York: Interscience, 1967, 2nd ed.,
- Sakurai, A. 1954, Journal of the Physical Society of Japan, 9, 256
- Sedov, L. I. 1959, Similarity and Dimensional Methods in Mechanics, New York: Academic Press, 1959
- Simionescu, A., Roediger, E., Nulsen, P. E. J., et al. 2009, A&A, 495, 721
- Soker, N. 2016, New Astron. Rev., 75, 1
- Tang, S., & Wang, Q. D. 2005, ApJ, 628, 205
- Taylor, G. I. 1946, Proceedings of the Royal Society of London Series A, 186, 273
- Truelove, J. K., & McKee, C. F. 1999, ApJS, 120, 299
- Xiang, F., Rudometkin, E., Churazov, E., Forman, W., Böhringer, H. 2009, MNRAS, 398, 575
- Zhuravleva I., et al., 2014, Nature, 515, 85
- Zhuravleva I., et al., 2016, MNRAS, 458, 2902

APPENDIX A:

The exact history of the mass and energy injection by an AGN during an outburst is not known from observation. In our simulations, we apply the following simplified prescription.

(i) All the mass M_{inj} is added at time $t = 0$ to a central region with radius $r_{ej}(0)$, so that the density of this region is

$$\rho[r < r_{ej}(0)] = \frac{3M_{inj}}{4\pi r_{ej}^3(0)}, \quad (\text{A1})$$

where $r_{ej}(0)$ is the ejecta radius at $t = 0$.

(ii) The energy is injected uniformly through this region over interval of time starting from $t=0$ to $t = t_b$ i.e.

$$\dot{e}(r, t) = \frac{3E_{inj}}{4\pi t_b r_{ej}^3(t)}, \quad 0 \leq t \leq t_b \quad (\text{A2})$$

where \dot{e} is the energy injection rate per unit mass per unit time. In simulations we typically consider the late phase evolution of an outburst, when the mass of the swept up gas is much larger than M_{inj} and the results are essentially insensitive to the value of M_{inj} , as long as the energy density in the ejecta, E_{inj}/M_{inj} , is much higher than the corresponding value of the ICM. With these parameters, the sound speed inside the ejecta is very high and eq. (A2) shall be a good assumption.

The adiabatic index of the injected plasma γ_{ej} is assumed to be the same as the ICM index $\gamma_a = 5/3$. While it is likely that the injected plasma is (at least partly) relativistic, suggesting $\gamma_{ej} \sim 4/3$, we are interested not in the internal structure of the ejecta, but rather in the structure of perturbations induced in the ICM by the outburst. These perturbations are not directly sensitive to the value of γ_{ej} , although the total energy E_{inj} required to generate the same perturbations does depend on γ_{ej} . For instance, in a slow outburst case (see discussion in Section 3.4), the total outburst energy is related to the volume of the ejecta $E_{inj} \approx \gamma_{ej}PV/(\gamma_{ej} - 1)$. As a result, a larger outburst energy E_{inj} is needed for smaller γ_{ej} in order to inflate a bubble with the same size.

APPENDIX B:

In this appendix, we constrain our discussion to a uniform ambient medium and instantaneous outburst with $t_b \rightarrow 0$ for simplification. We consider an outburst with total injected energy E_{inj} and total injected mass M_{inj} in an ambient medium with density ρ_a and pressure P_a under spherical symmetry. We assume the energy and mass of the swept materials as $E_{sw} = 4\pi P_a R^3/3(\gamma_a - 1)$ and $M_{sw} = 4\pi\rho_a R^3/3$ respectively, where γ_a is the adiabatic index of the ambient medium and R is the radius of the outburst. At early time, when $E_{sw}/E_{inj} \ll 1$ and $M_{sw}/M_{inj} \ll 1$, the surrounding medium is not important. The expansion of the outburst is only determined by E_{inj} and M_{inj} , and characterized by free expansion with $R \propto \sqrt{E_{inj}/M_{inj}t_{age}}$ according to dimensional analysis. As the age t_{age} increases, the evolution of an outburst could fall into two different regimes depending

on the dimensionless ratio

$$\begin{aligned} w &= \frac{E_{inj}M_{sw}}{E_{sw}M_{inj}} = \frac{(\gamma_a - 1)E_{inj}\rho_a}{M_{inj}P_a} \\ &= 5 \times 10^4 (\gamma_a - 1) \left(\frac{E_{inj}}{10^{57} \text{erg}} \right) \left(\frac{10^3 M_\odot}{M_{inj}} \right) \\ &\times \left(\frac{\rho_a}{0.1 m_p \text{cm}^{-3}} \right) \left(\frac{1 \text{keV cm}^{-3}}{P_a} \right) \end{aligned} \quad (\text{B1})$$

where m_p is the proton mass.

In the first regime with $w \gtrsim 1$, the outburst could enter a phase with $E_{sw}/E_{inj} \ll 1$ and $M_{sw}/M_{inj} \gtrsim 1$ in which the injected mass M_{inj} and the pressure P_a of the ambient medium are not very important. The expansion of the outburst is only determined by E_{inj} and ρ_a , and characterized by the relation $R \propto (E_{inj}t_{age}^2/\rho_a)^{1/5}$ according to dimensional analysis. This is simply the classic ST solution. As t_{age} further increases, eventually we have $E_{sw}/E_{inj} \gtrsim 1$ and $M_{sw}/M_{inj} \gg 1$. Now the outburst starts to lose the memory of E_{inj} . The expansion of the outburst is only determined by P_a and ρ_a , and characterized by the relation $R \propto \sqrt{P_a/\rho_a}$ according to dimensional analysis. This is of course the sound wave solution. So in the first regime, the outburst initially expands freely and then transits to the classic ST solution. As t_{age} further increases, the strong shock eventually becomes a weak shock and asymptotically approaches a sound wave. In the second regime with $w \lesssim 1$, the classic ST solution is no longer available for the system. Instead the outburst will enter a phase with $E_{sw}/E_{inj} \gtrsim 1$ and $M_{sw}/M_{inj} \ll 1$, which is very unstable to Rayleigh-Taylor instability.

In most astrophysical applications like AGN feedback problem here, the evolution of the system falls into the first regime with $w \gg 1$. However in extreme condition, e.g. supernova explosion in AGN driven bubble (Chugai et al. 2011), the evolution of the object could enter the second regime.

APPENDIX C:

In this appendix, we constrain our discussion to a uniform ambient medium for simplification. For a non-uniform medium we could replace the pressure and density in the following discussion with volume averaged values. For the AGN feedback problem of interest here, M_{inj} is negligible and the intrinsic properties of an outburst are characterized by only E_{inj} and t_b . E_{inj} sets the characteristic scales for an outburst. Let's assume R_E satisfy

$$E_{inj} = \frac{4\pi}{3} P_a R_E^3 \quad (\text{C1})$$

where P_a is the pressure in the ambient medium. R_E depends on both the intrinsic properties of an outburst, i.e. E_{inj} , and the physical properties of the surrounding ambient medium, i.e. $P_a(r)$. The corresponding time scale for R_E is simply the sound crossing time

$$t_E = R_E \sqrt{\rho_a/\gamma_a P_a}, \quad (\text{C2})$$

where ρ_a is the ambient density.

For typical parameters of an outburst, we have

$$R_E = \left(\frac{3E_{inj}}{4\pi P_a} \right)^{1/3} = 1.7 \text{ kpc} \left(\frac{E_{inj}}{10^{57} \text{erg}} \right)^{1/3} \left(\frac{1 \text{keV cm}^{-3}}{P_a} \right)^{1/3}$$

(C3)

and

$$t_E = \frac{(3E_{inj})^{1/3} \rho_a^{1/2}}{(4\pi)^{1/3} \sqrt{\gamma_a} P_a^{5/6}} = 1.33 \text{ Myr } \mu^{1/2} \left(\frac{E_{inj}}{10^{57} \text{ erg}} \right)^{1/3} \\ \times \left(\frac{n}{0.1 \text{ cm}^{-3}} \right)^{1/2} \left(\frac{1 \text{ keV cm}^{-3}}{P_a} \right)^{5/6}, \quad (\text{C4})$$

where n is the number density of the surrounding medium and μ is the mean molecular weight. Through the paper, we assume $\mu = 0.6$ for fully ionized medium with solar abundance.

If the energy injection rate L within t_b is constant as assumed in this paper, i.e. $E_{inj} = Lt_b$, then for a continuous outburst, t_E in the above discussion is equivalent to

$$t_L = \frac{(3L)^{1/2} \rho_a^{3/4}}{\sqrt{4\pi} \gamma_a^{3/4} P_a^{5/4}} = 8.6 \text{ Myr } \mu^{3/4} \left(\frac{L}{10^{45} \text{ ergs}^{-1}} \right)^{1/2} \\ \times \left(\frac{n}{0.1 \text{ cm}^{-3}} \right)^{3/4} \left(\frac{1 \text{ keV cm}^{-3}}{P_a} \right)^{5/4}. \quad (\text{C5})$$

and $t_L = t_E^{3/2}/t_b^{1/2}$. It characterizes the time when energy stored in the material swept up per unit time becomes comparable with the energy injection rate L . The corresponding length scale is

$$R_L = \frac{(3L)^{1/2} \rho_a^{1/4}}{\sqrt{4\pi} \gamma_a^{1/4} P_a^{3/4}} = 11.1 \text{ kpc } \mu^{1/4} \left(\frac{L}{10^{45} \text{ ergs}^{-1}} \right)^{1/2} \\ \times \left(\frac{n}{0.1 \text{ cm}^{-3}} \right)^{1/4} \left(\frac{1 \text{ keV cm}^{-3}}{P_a} \right)^{3/4}. \quad (\text{C6})$$

APPENDIX D:

We use a one dimensional hydrodynamical code described in the Appendix B of [Truelove & McKee \(1999\)](#) to simulate the problem. It uses a Lagrangian finite differencing scheme with standard formulation of artificial viscosity as discussed in [Richtmyer & Morton \(1967\)](#). We replaced the artificial viscosity with

$$q = \rho \left\{ c_2 \frac{\gamma+1}{4} |\Delta v| + \sqrt{c_2^2 \left(\frac{\gamma+1}{4} \right)^2 \Delta v^2 + c_1^2 c_s^2} \right\} |\Delta v| \quad (\text{D1})$$

to achieve better performance for weak shocks. Δv is the velocity jump across a zone, ρ is the density of the zone and c_s is the sound speed in the zone ([Caramana et al. 1998](#)). $c_1 = 0.5$ and $c_2 = 1$ are applied in the simulation to constrain the shock region within a few zones. A Lagrangian CFL condition is utilized in all the simulation with CFL number of 0.5 and the increase of the time step is required to be no more than 5% between steps. Various parameters used in the simulation of an outburst in a uniform medium are presented in Table D1. We solve the hydrodynamic equa-

Table D1. Basic parameters for numerical simulations of an outburst in a uniform ambient medium

injected mass M_{ej}	$1000 M_\odot$
outburst energy E_{inj}	10^{57} erg
ambient density n_a	0.1 cm^{-3}
ambient pressure P_a	1 keV cm^{-3}

tions in the Lagrangian form

$$\frac{\partial r}{\partial t} = v, \quad (\text{D2})$$

$$\frac{\partial v}{\partial t} = -4\pi r^2 \left(\frac{\partial P}{\partial M} + \rho \frac{\partial \phi}{\partial M} \right), \quad (\text{D3})$$

$$\frac{\partial e}{\partial t} = \frac{P}{\rho^2} \frac{\partial \rho}{\partial t} + \dot{e}, \quad (\text{D4})$$

$$\frac{\partial}{\partial M} \left(\frac{4\pi r^3}{3} \right) = \frac{1}{\rho}, \quad (\text{D5})$$

$$(\text{D6})$$

where e is the internal energy per unit mass and ϕ is the gravitational potential. A static gravitational potential is assumed in the simulation and is derived by solving the hydrostatic equilibrium in the hot media at $t = 0$,

$$\frac{1}{\rho} \frac{dP}{dr} = -\frac{d\phi}{dr}. \quad (\text{D7})$$

The mass injected in the simulation corresponds to a ratio $E_{inj} \rho_a / M_{inj} P_a \sim 10^{-4}$, see detailed discussion in Appendix B. A slight change of M_{ej} could affect the density and temperature profile around the central ejecta bubble slightly while the outer structure of the outburst shall remain unchanged.

APPENDIX E:

In this Appendix, we discuss the shock evolution in an instantaneous outburst and a continuous outburst. For simplification, we assume a uniform ambient medium.

In [Tang & Wang \(2005\)](#), it has been shown that in an instantaneous outburst the shock velocity V_s could be reproduced within 3 percent accuracy by simply connecting the ST solution velocity and the sound speed in the ambient medium as follows

$$V_s(t) = \left(V_{ST}^{5/3}(t) + c_s^{5/3} \right)^{3/5} = c_s \left(1 + \eta \frac{t_E}{t} \right)^{3/5}, \quad (\text{E1})$$

where V_{ST} is the velocity from the ST solution, c_s is the sound speed in the ambient medium and $\eta = (2\xi/5)^{5/3} (4\pi/3\gamma_a)^{1/3} \approx 0.374$ for $\gamma_a = 5/3$ and $\xi = 1.152$. At $t = t_E$, we have $M \approx 1.2$ which implies t_E characterizing the transition from strong shock to weak shock.

We can rewrite eq E1 to express the shock age as a function of Mach number, i.e.

$$t = \frac{\eta t_E}{M^{5/3} - 1}. \quad (\text{E2})$$

The above equation can be used to estimate the age of an instantaneous outburst based on the known Mach number.

The radius of the shock front R_s could be derived by integrating the velocity V_s and after some calculation we

obtain

$$R_s(t) = \frac{5}{2} c_s \eta t_E \left(\frac{t}{\eta t_E} \right)^{2/5} F\left(-\frac{3}{5}, \frac{2}{5}; \frac{7}{5}; -\frac{t}{\eta t_E}\right) \quad (\text{E3})$$

which is equivalent to eq (4) in [Tang & Wang \(2005\)](#) and F is the generalized hypergeometric function.

The dynamical evolution of a continuous outburst with a constant energy injection rate L and negligible ambient pressure can be described by a generalized ST solution ([Dokuchaev 2002](#)), in which the shock radius and velocity follow

$$R_{GST} = \xi_L \left(\frac{Lt^3}{\rho} \right)^{1/5} \quad \text{and} \quad V_{GST} = \frac{dR}{dt} = \frac{3\xi_L}{5} \left(\frac{L}{\rho t^2} \right)^{1/5} \quad (\text{E4})$$

respectively. ξ_L is a dimensionless constant and for $\gamma_a = 5/3$ [Dokuchaev \(2002\)](#) found $\xi_L = 0.929$. Although the generalized ST solution provided in [Dokuchaev \(2002\)](#) requires a special distribution of energy injection in space which is different from our numerical set up, we find the solution provides a good fit to the simulation results for the time range investigated in this paper.

Following the idea in [Tang & Wang \(2005\)](#) for an instantaneous outburst, we find the velocity of a continuous outburst with constant energy injection rate L can be approximated by connecting the generalized ST solution velocity and the sound speed together as follows

$$V_s(t) = \left(V_{GST}^{5/2}(t) + c_s^{5/2} \right)^{2/5} = c_s \left(1 + \eta_L \frac{t_L}{t} \right)^{2/5} \quad (\text{E5})$$

where $\eta_L = (3\xi_L/5)^{5/2} (4\pi/3\gamma_a)^{1/2} \approx 0.368$ for $\gamma_a = 5/3$. We can rewrite eq. [E5](#) to express the shock age as a function of Mach number, i.e.

$$t = \frac{\eta_L t_L}{M^{5/2} - 1}. \quad (\text{E6})$$

The above equation can be used to estimate the age of a continuous outburst at arbitrary Mach M .

The corresponding shock radius can be obtained by integrating eq. [E5](#) over time. After some calculation we get

$$R_s(t) = \frac{5}{3} c_s \eta_L t_L \left(\frac{t}{\eta_L t_L} \right)^{3/5} F\left(-\frac{2}{5}, \frac{3}{5}; \frac{8}{5}; -\frac{t}{\eta_L t_L}\right) \quad (\text{E7})$$

which can reproduce the simulation results within a few percent. F again is the generalized hypergeometric function.

For a continuous outburst, at late times when $t_{age} \gtrsim t_E$, the energy left in ejecta is $E_{ej} = Lt_{age}/\gamma_{ej} = PV/(\gamma_{ej} - 1)$. The corresponding ejecta radius then becomes

$$R_{ej}(t) = \left[\frac{3(\gamma_{ej} - 1)Lt}{4\pi\gamma_{ej}P} \right]^{1/3} = R_L \left[\frac{3(\gamma_{ej} - 1)t}{4\pi\gamma_{ej}t_L} \right]^{1/3}. \quad (\text{E8})$$

According to eq [E7](#) and [E8](#), the R_s/R_{ej} ratio for a continuous outburst at $t_{age} \gtrsim t_E$ simply satisfies

$$\begin{aligned} \frac{R_s(t)}{R_{ej}(t)} &= \xi_L \left(\frac{4\pi}{3\gamma_a} \right)^{1/5} \left[\frac{\gamma_{ej}}{\gamma_{ej} - 1} \right]^{1/3} \\ &\times \left(\frac{t}{t_L} \right)^{4/15} F\left(-\frac{2}{5}, \frac{3}{5}; \frac{8}{5}; -\frac{t}{\eta_L t_L}\right) \end{aligned} \quad (\text{E9})$$

where $\eta_L = (3\xi_L/5)^{5/2} (4\pi/3\gamma_a)^{1/2} \approx 0.368$ and $\xi_L = 0.929$

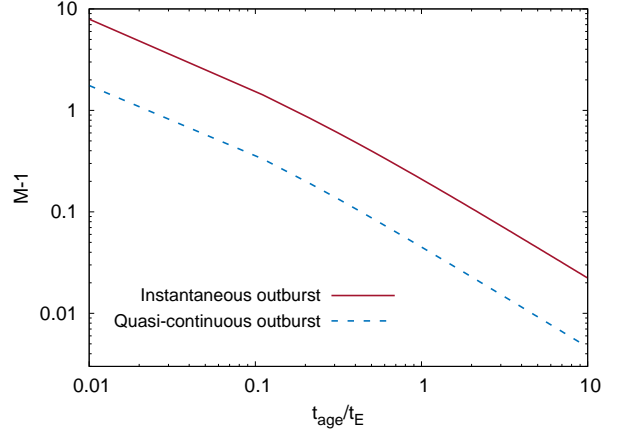


Figure E1. $M-1$ as a function of t_{age}/t_E according to analytical approximation eq. [E1](#) and [E5](#). Red solid line is for an instantaneous outburst and the blue dashed line is for a quasi-continuous outburst with $t_b = 10t_E$.

for $\gamma_a = 5/3$ ([Dokuchaev 2002](#)). F again is the generalized hypergeometric function.

[Fig. E1](#) illustrates how the Mach number decrease with time for both an instantaneous outburst and a quasi-continuous outburst with $t_b/t_E = 10$ based on analytical approximations derived in this Appendix. As t_b/t_E gradually increases, i.e. longer outbursts, the value of $M-1$ will decrease even faster accordingly. Thus a quasi-continuous outburst with $t_b/t_E \gg 1$ is characterized by a weak shock propagating at essentially the sound speed over almost the entire duration of the outburst.

APPENDIX F:

The unperturbed density and temperature distribution adopted in our simulation for M87 and the Perseus cluster are presented as below.

In M87 ([Xiang et al. 2009](#))

$$n_e(r) = 0.22 \text{ cm}^{-3} \left[1 + \left(\frac{r}{r_c} \right)^2 \right]^{-3\beta/2} \quad (\text{F1})$$

where $\beta = 0.33$ and $r_c = 0.93 \text{ kpc}$ and

$$T_e(r) = 1.55 \text{ keV} \left[1 + \left(\frac{r}{10.23 \text{ kpc}} \right)^2 \right]^{0.18}. \quad (\text{F2})$$

The total number density to electron number density ratio, i.e. n_t/n_e , is assumed to be 1.9 through the paper. A static gravitational potential is assumed in the simulation and solved by requiring that the ambient medium satisfy hydrostatic equilibrium.

For the Perseus cluster, we adopted a slightly modified version of the profiles from [Churazov et al. \(2003\)](#), re-scaled to a Hubble constant of 70 km/s/Mpc .

$$n_e(r) = \frac{5.36 \times 10^{-2} \text{ cm}^{-3}}{[1 + (r/55 \text{ kpc})^2]^{1.8}} + \frac{4.6 \times 10^{-3} \text{ cm}^{-3}}{[1 + (r/200 \text{ kpc})^2]^{0.87}} \quad (\text{F3})$$

and

$$T_e(r) = 9.0 \text{keV} \frac{1 + (r/60 \text{kpc})^{2.5}}{2.7 + (r/60 \text{kpc})^{2.6}}. \quad (\text{F4})$$

The best fit simulation results for the Perseus cluster and M87 are presented in Fig. F1 and F2 respectively, which are consistent with previous discussion in Zhuravleva et al. (2016) and Forman et al. (2017). According to the above simulations, it is interesting to see that the Perseus cluster seems to have ongoing energy injection for quite a long time until now, while the AGN activity in M87 seems to be quenched a long time ago. As a result, the outbursts in the Perseus cluster and M87 show quite different dynamical structures.

The continuous outburst in the Perseus cluster mainly consists two parts, a hot ejecta bubble and a WSH gas envelope, which are the same as that in a uniform medium (see Fig. 4). The WSH envelope in the Perseus cluster has physical properties close to the unperturbed ambient medium except the region close to the shock front, which is also similar to outbursts in a uniform medium. A significant amount of energy, more than 50% of E_{inj} , is stored in the central ejecta bubble, which is consistent with a continuous outburst in a uniform medium. No WLS appears in the WSH envelope as the energy injection driving such an outburst hasn't quenched yet. Only about 2% of injected energy E_{inj} is transferred to the gravitational energy, which indicates the surrounding medium swept up by the shock front doesn't deviate too much from a uniform distribution.

The simulation results for M87 are presented in Fig. F2 and are consistent with that from an intermediate outburst in a uniform medium. The spatial structure of the outburst also contains two parts, a central ejecta bubble and a WSH gas envelope. But the WSH envelope in M87 is dominated by the WLS while the structure between R_{env} and R_w (see Fig. 3 for example), which has physical properties close to the unperturbed medium, is negligible in the figure. It implies that the t_{age}/t_E ratio in M87 is not very large and the WLS structure has just detached from the central ejecta bubble. The energy stored in the ejecta bubble of M87 is smaller than the Perseus cluster and is about 30% which is consistent with an intermediate outburst. In the mean time, about 50% of the injected energy E_{inj} is transferred to the gravitational energy due to the steep density profile in the core of M87. As a result, the time evolution of various energy components in M87 becomes more complicated than that in a uniform medium as the surrounding environment now has a strong effect in shaping the dynamical structure of the outburst.

Overall the spatial structure of an outburst in a non-uniform medium is qualitatively similar to that in the uniform medium.

APPENDIX G:

In this Appendix, we investigate the validity of Fig. 8 and show that the contours in the figure derived with simulation in a uniform medium are still a good approximation for AGN driven outbursts in galaxies and clusters with non-uniform media. In a non-uniform medium, the effective characteristic time t_E depends on the spatial structure of the ambient medium and evolves with time during the evolution.

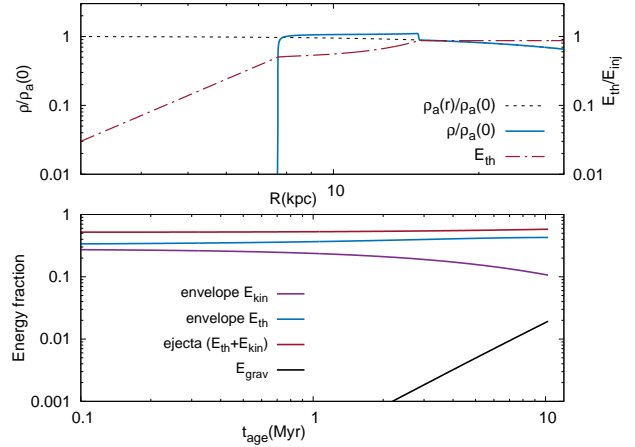


Figure F1. Numerical simulation for an outburst in the Perseus cluster with total injected energy $E_{inj} \approx 1.1 \times 10^{59}$ erg energy and $t_b = t_{age} = 10.3$ Myrs. The upper panel shows the normalized density distribution (red solid) and the accumulative thermal energy distribution E_{th} (dotted blue). The dashed green line is the normalized unperturbed density distribution. The lower panel presents the time evolution of the different energy components during the expansion of an outburst.

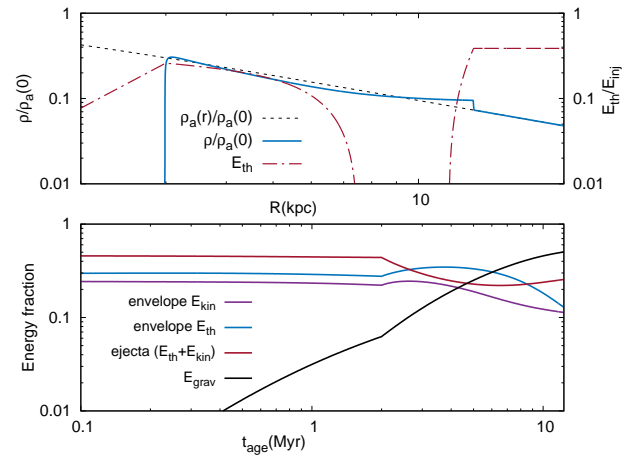


Figure F2. Numerical simulation for an outburst in M87 with total injected energy $E_{inj} = 5.5 \times 10^{57}$ erg, outburst duration time $t_b = 2$ Myrs and age $t_{age} = 12.3$ Myr. The upper panel shows the normalized density distribution (blue solid) and the accumulative thermal energy distribution E_{th} (red dotted dashed). The dotted black line is the normalized unperturbed density distribution. The lower panel presents the time evolution of different energy components during the expansion of an outburst.

As a result, different clusters or galaxies with different density and pressure profile exhibit different foot prints in Fig. 8. Therefore it is impossible to make a complete comparison between the uniform medium case and the non-uniform medium case. We instead use M87 and the Perseus cluster as examples to illustrate possible difference between the uniform medium and non-uniform medium simulation results. As we will show later, for galaxy clusters with shallow den-

sity and pressure profile (power law index $\lesssim 2$) like M87 and the Perseus cluster, the deviation from a uniform medium results is not very significant and Fig. 8 can still be considered as a good approximation for AGN driven outbursts in galaxies and clusters with non-uniform media.

In Fig. G1, we present the contours of t_b/t_E (blue solid) as a function of $G = P_s R_s^3 / P_{ej} R_{ej}^3$ and $M - 1$ based on simulation in a uniform medium. We also plot two curves, one for a short outburst and the other for a long outburst, with both the Perseus cluster (black dotted-dashed) and M87 (red dashed) profiles to compare the non-uniform medium results with uniform medium ones. The short outburst is simulated with $t_b/t_E = 0.02$, where t_E is calculated with pressure and density in the center of the galaxy. The long outburst chosen for illustration is our best fit numerical model for the two objects shown in Table 2.

The black dotted-dashed curves with density and pressure profile of the Perseus cluster agree with the corresponding uniform medium lines very well. It is mainly because the core of Perseus cluster has very flat density and pressure profile. Moreover, for the time and Mach number range we are interested in the outburst mainly expands in the flat core with an almost uniform medium and hasn't reached the steep envelope of the galaxy yet. The red dashed curves in M87 profiles show larger deviation from the uniform medium lines. At early times with $M \sim 2$, we found the curves for M87 fall below the corresponding uniform medium line. This is mainly because the temperature profile in M87 increases with radius instead of decreasing with radius which is different from the Perseus cluster. Because of this, the pressure profile in M87 exhibits a broken power law distribution with a steeper power in the inner part and a shallower power law in the outer part. The break happens at around 10kpc. When the shock front is in the shallower power law region while the ejecta bubble is in the steep power law region, the $P_s R_s^3 / P_{ej} R_{ej}^3$ ratio can decrease with time and become smaller than the uniform medium results. The two simulations of M87 are stopped with shock radius about 15kpc which indicates the outburst indeed pass through this region during the expansion. As time increases and M decreases, the curves start to bend up and approach the uniform medium line with smaller t_b/t_E ratios. It is because the outburst enters the envelope of M87 with a steeper profile. The pressure and density are decreasing with radius very quickly in the envelope. As a result, the characteristic time t_E is increasing with time and the effective t_b/t_E of the outburst is decreasing with time which cause the curves to bend up.

Although the curves for the Perseus cluster and M87 behave slightly differently due to the different density and temperature distributions. For the Mach number range 1.1 – 1.3 and t_b/t_E ratio between 0.01 and 1, which we are particularly interested in, the deviation is not very significant. Thus the contours derived in simulation with a uniform medium are still a good approximation for AGN driven outbursts in galaxies and clusters with shallow density and pressure profiles (power law index $\lesssim 2$).

This paper has been typeset from a $\text{\TeX}/\text{\LaTeX}$ file prepared by the author.

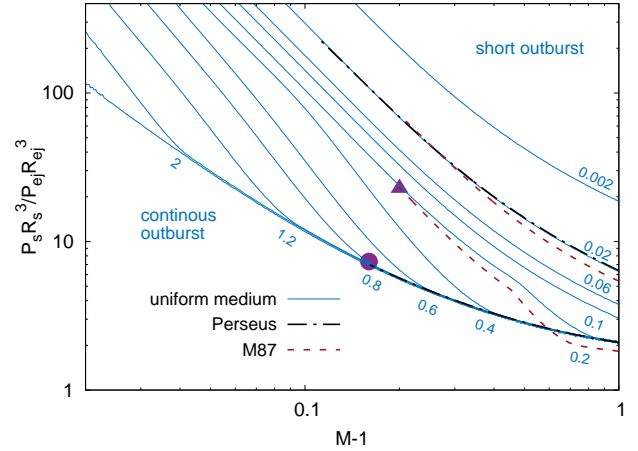


Figure G1. x axis: $M - 1$ where M is the Mach number of the shock wave; y axis: $G = P_s R_s^3 / P_{ej} R_{ej}^3$ where R_s is the shock radius, R_{ej} is the ejecta radius, P_{ej} is the pressure at R_{ej} and P_s is the pressure at R_s . Blue solid lines represent the contours with different t_b/t_E derived in a uniform medium. Blue numbers mark the corresponding t_b/t_E ratio of the line. The bottom blue solid line can be considered as a representative of a continuous outburst. Black dotted-dashed lines are for the Perseus cluster while red dashed lines are for M87. For both the Perseus cluster and M87, the upper curves presented are short outbursts with $t_b/t_E = 0.02$ (t_E is calculated from the density and pressure in the galaxy center) and the lower curves show our best fit numerical models as examples for long outbursts.